
MINGLE: Mixtures of Null-Space Gated Low-Rank Experts for Test-Time Continual Model Merging

Zihuan Qiu¹ Yi Xu² Chiyuan He¹ Fanman Meng¹
 Linfeng Xu¹ Qingbo Wu¹ Hongliang Li¹

¹University of Electronic Science and Technology of China, Chengdu, China

²Dalian University of Technology, Dalian, China

Abstract

Continual model merging integrates independently fine-tuned models sequentially without access to original training data, providing a scalable and efficient solution to continual learning. However, current methods still face critical challenges, notably parameter interference among tasks and limited adaptability to evolving test distributions. The former causes catastrophic forgetting of integrated tasks, while the latter hinders effective adaptation to new tasks. To address these, we propose MINGLE, a novel framework for test-time continual model merging, which leverages test-time adaptation using a small set of unlabeled test samples from the current task to dynamically guide the merging process. MINGLE employs a mixture-of-experts architecture composed of parameter-efficient, low-rank experts, enabling efficient adaptation and improving robustness to distribution shifts. To mitigate catastrophic forgetting, we propose Null-Space Constrained Gating, which restricts gating updates to subspaces orthogonal to prior task representations. This suppresses activations on old task inputs and preserves model behavior on past tasks. To further balance stability and adaptability, we design an Adaptive Relaxation Strategy, which dynamically adjusts the constraint strength based on interference signals captured during test-time adaptation. Extensive experiments on standard continual merging benchmarks demonstrate that MINGLE achieves robust generalization, reduces forgetting significantly, and consistently surpasses previous state-of-the-art methods by 7-9% on average across diverse task orders.

1 Introduction

Continual learning seeks to incrementally adapt machine learning models to new tasks without forgetting previously learned knowledge, addressing the critical challenge of catastrophic forgetting [41]. However, conventional continual learning approaches typically require continuous access to original training data, raising significant concerns about privacy and substantial computational overhead due to retraining efforts, thus limiting their applicability in dynamic, data-sensitive environments.

To address these limitations, recent works have explored an alternative paradigm known as continual model merging (CMM), which sequentially integrates independently fine-tuned models directly in parameter space, without revisiting any past training data [37, 49, 68]. CMM typically operates under a "merge-to-transfer" paradigm: given a pretrained model θ_0 and independently fine-tuned models $\{\theta_t\}_{t=1}^T$, a unified model is constructed by combining task-specific weight updates $\Delta\theta_t = \theta_t - \theta_0$ via weighted averaging or projection-based strategies [23, 77, 67].

Despite its advantages in scalability, data privacy, and distributed training capabilities [42, 13, 55], existing CMM methods still encounter critical issues, notably severe parameter interference between tasks and limited adaptability to evolving test distributions. This parameter interference arises because, as fine-tuned models are incrementally merged, overlapping or conflicting parameter

updates accumulate, resulting in severe forgetting of previously learned tasks. To mitigate this interference, recent methods introduce structural constraints such as orthogonal projection [68, 74], model linearization [37, 67], and pruning-based sparsification [82, 86]. However, their effectiveness diminishes as task count grows and interference becomes increasingly entangled. Moreover, models merged across tasks often fail to generalize effectively, particularly when facing unseen or shifting task conditions. These flaws result in severe forgetting of earlier tasks and substantial performance gaps compared to the upper bound achieved by individually fine-tuned models. As shown in Fig. 1, TA [23] suffers from large performance gaps and strong forgetting, reflected by low accuracy and negative backward transfer (BWT). OPCM [68] improves over TA via orthogonalized merging but still shows notable degradation.

To overcome these limitations, we propose a novel continual merging paradigm—**Test-Time Continual Model Merging (TTCMM)**—which explicitly introduces the concept of test-time adaptation (TTA) [72, 61] into model merging. Unlike prior TTA-based multi-task merging methods [83, 66, 84], which assume simultaneous availability of models and test data from all tasks, TTCMM utilizes only a small set of unlabeled samples from the current task, making it uniquely suited for realistic continual scenarios where revisiting historical data is often infeasible.

In this paper, we propose **MINGLE (MIxtures of Null-Space Gated Low-rank Experts)**, a method designed to continually merge independently fine-tuned models at test-time while preserving prior knowledge. MINGLE employs a mixture-of-experts architecture [26, 43] composed of lightweight LoRA-based [20] experts, enabling efficient and flexible test-time adaptation. To robustly prevent interference from previously learned tasks, we introduce a novel **Null-Space Constrained Gating** mechanism, restricting gating updates to task-orthogonal subspaces. Additionally, we propose an **Adaptive Relaxation Strategy** to dynamically modulate constraint strength based on test-time interference feedback during adaptation.

Extensive experiments on standard continual learning benchmarks show that MINGLE consistently outperforms previous state-of-the-art approaches by 7–9% on average, achieving robust generalization and strong resistance to catastrophic forgetting across diverse continual learning scenarios. Remarkably, these improvements are achieved entirely without any access to original training data, demonstrating the effectiveness of our TTCMM paradigm and the power of test-time adaptation in continual learning.

Our contributions are summarized as follows:

- We formalize test-time continual model merging (TTCMM), a novel framework leveraging unlabeled test samples for merging independently fine-tuned models.
- We propose MINGLE, a TTCMM method with Adaptive Null-Space Constrained Gating to effectively balance stability and plasticity.
- Extensive experiments show that MINGLE achieves state-of-the-art performance, consistently outperforming prior methods in accuracy, robustness and resistance to forgetting.

2 Related Work

Continual Learning. Continual learning (CL) aims to mitigate catastrophic forgetting [41], where models forget prior tasks when learning new ones. Regularization-based methods constrain updates via importance weights [30, 88, 2, 29, 78], while distillation techniques preserve knowledge by aligning outputs or intermediate features [19, 11, 58, 50]. Replay-based methods store exemplars or generate surrogates using prompts, prototypes, or generators [53, 38, 75, 59, 51]. Dynamic architectures expand capacity through growth or ensembling [34, 94, 40]. Recent work integrates lightweight adapters or prompts into pre-trained models to enhance transfer with minimal updates [85, 22, 76]. CL has also been approached through model merging [77, 23, 27, 66]. One line remains close to conventional CL, incrementally fine-tuning models and merging them to reduce forgetting [39, 40, 15]. These methods typically require access to training data and involve *sequential task-wise fine-tuning*. In contrast, the continual model merging paradigm [27, 37, 5, 49, 68] merges *independently fine-tuned models* without revisiting prior data, offering greater scalability and privacy.

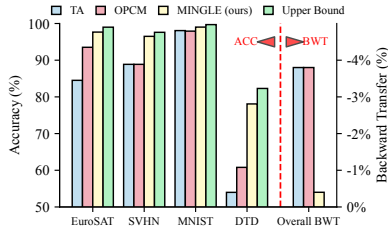


Figure 1: Performance after eight task continual merging: accuracy on first four tasks and overall BWT.

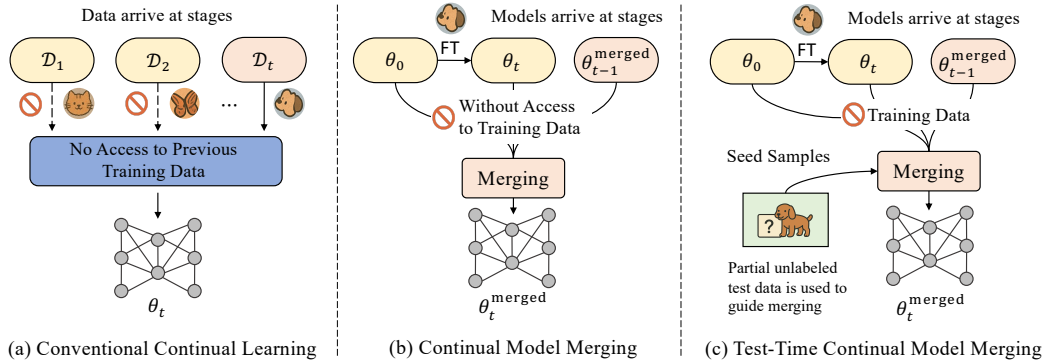


Figure 2: Comparison of three continual learning paradigms. (a) Conventional Continual Learning trains models sequentially with data arriving in stages, without access to previous task data. (b) Continual Model Merging continually fuses independently trained models, without access to any training data. (c) Test-Time Continual Model Merging improves merging by leveraging a few unlabeled test samples from the current task.

Model Merging. Early work merged models via direct parameter averaging [70, 56], later refined by linear mode connectivity [12, 1]. Task Arithmetic (TA) [23] generalizes this by viewing models as task vectors to be summed. However, TA relies on weight disentanglement [47], which standard fine-tuning often violates, prompting structured training [27, 63]. Beyond averaging, interference-aware methods reweight or sparsify parameters [82, 86], or fuse models via distillation and clustering [83, 73]. LoRA-based tuning [20] introduces additional challenges due to parameter entanglement, spurring gradient-free or retrieval-based fusion strategies [21, 90, 91].

Test-Time Adaptation. TTA updates models at inference to counter test-time distribution shift. Early methods employed self-supervised objectives [64], entropy minimization [72], and regularized updates [61]. Online TTA adapts continuously [24], while batch-wise variants ignore temporal structure [16]. To improve stability, recent methods incorporate confidence filtering [46], EMA [10], partial updates [87], test-time augmentation [89], and adaptive BatchNorm [54]. In vision–language models, TTA leverages prompts or adapters [57, 14, 35]. Our approach draws on TTA to steer merging dynamics, aligning fused models with continuously evolving test distributions.

Discussion. Most related to our method are MoE-Adapter [85] and WEMOE [66], both leveraging MoE architectures [26, 28]. MoE-Adapter follows conventional CL, where expert modules are embedded in the model and trained as a whole across tasks. In contrast, we adopt a model merging paradigm: experts are extracted from independently fine-tuned models and inserted without training. While WEMOE incorporates TTA, it is designed for multitask learning rather than continual scenarios, relying on simultaneous access to all models and data. By contrast, MINGLE is explicitly tailored for the more challenging continual merging setup.

3 MINGLE: Mixtures of Null-Space Gated Low-Rank Experts

3.1 Preliminaries

Problem Setting. We study continual learning in a model merging setting, where a sequence of task-specific models $\{\theta_1, \dots, \theta_T\}$ are independently fine-tuned from a shared pre-trained model θ_0 , each using a dataset $\mathcal{D}_i = \{(x_j^{(i)}, y_j^{(i)})\}$ with label space $\mathcal{C}_i \subset \mathcal{Y}$. The goal is to construct a unified model θ_T^{merged} that generalizes across the combined label space $\mathcal{C}_{1:T} = \bigcup_{i=1}^T \mathcal{C}_i$.

Unlike conventional continual learning, we assume no access to training data during merging. All adaptation happens directly in parameter space. This paradigm is relevant in scenarios where only final fine-tuned models are retained, while original training data is discarded due to privacy, storage, or accessibility constraints.

To contextualize this, we compare with two related paradigms in Fig. 2:

- **Conventional Continual Learning.** A single model θ is sequentially updated on $\mathcal{D}_1, \dots, \mathcal{D}_T$, discarding previous data. It requires direct training data access and extensive retraining.

- **Continual Model Merging.** A sequence of models $\{\theta_i\}$ are merged incrementally in parameter space without access to training data and earlier models: $\theta_t^{\text{merged}} = \text{Merge}(\theta_{t-1}^{\text{merged}}, \theta_t)$.
- **Test-Time Continual Model Merging.** An extension of the above where a small unlabeled subset $\mathcal{D}_t^{\text{seed}} \subset \mathcal{D}_t^{\text{test}}$ (e.g., 5 samples per class) is available at each stage to provide lightweight task-specific guidance. We refer to $\mathcal{D}_t^{\text{seed}}$ as the *seed samples* of task t .

Existing Continual Merging Strategies. Let θ_0 denote the parameters of a pre-trained model. The corresponding task vector is defined as $\Delta\theta_t = \theta_t - \theta_0$.

- **Continual Task Arithmetic (C. TA).** A simple additive merge [23]: $\theta_t^{\text{merged}} = \theta_{t-1}^{\text{merged}} + \lambda\Delta\theta_t$, where λ is a scalar. While training-free, it is sensitive to λ and prone to task interference.
- **Orthogonal Projection-based Continual Merging (OPCM).** Tang et al. [68] propose projecting each $\Delta\theta_t$ onto the orthogonal complement of previous directions: $\theta_t^{\text{merged}} = \theta_0 + \frac{1}{\lambda_t} \left[\lambda_{t-1} \Delta\theta_{t-1}^{\text{merged}} + \mathcal{P}^{(t-1)}(\Delta\theta_t) \right]$, where $\mathcal{P}^{(t-1)}$ retains components orthogonal to previous updates. This reduces interference but ignores adaptation to task distributions.

To address these issues, we present MINGLE, which leverages $\mathcal{D}_t^{\text{seed}}$ to modulate the integration of θ_t at test-time, enhancing alignment to test distribution and mitigating task interference.

3.2 Motivation and Theoretical Analysis

Most existing continual model merging methods combine fine-tuned models via static averaging, where each expert is assigned fixed coefficients, thereby enforcing the *same* mixing rule across the whole input space. Consequently, it cannot specialize to regions where one expert is clearly superior. In contrast, a Mixture-of-Experts (MoE) equips every input with a *data-dependent* gate $g(x) = (g_1(x), \dots, g_T(x))$ that selects or re-weights experts on-the-fly. We give a formal comparison between static averaging and dynamic MoE under a noisy-routing scenario.¹

Theorem 1 (Dynamic MoE versus Static Averaging). *Let $\{(D_t, f_t)\}_{t=1}^T$ be T independent tasks with priors $P(t)$ and per-task risks $R_t(i)$. For any static mixture $h_{\text{static}}(x) = \sum_{i=1}^T \alpha_i f_i(x)$ and any hard-routed MoE $h_{\text{MoE}}(x) = f_{i^*(x)}(x)$ with task-specific routing errors ε_t :*

$$R(h_{\text{MoE}}) = R_{\text{ideal}} + \sum_{t=1}^T P(t) \varepsilon_t (R_{\text{wrong},t} - R_t(t)), \quad (1)$$

where $R_{\text{ideal}} = \sum_t P(t) R_t(t)$ and $R_{\text{wrong},t} = \frac{1}{T-1} \sum_{i \neq t} R_t(i)$. Moreover,

1. (Perfect routing) If $\varepsilon_t = 0$ for all t , then $\inf_g R(h_{\text{MoE}}) < \inf_{\alpha} R(h_{\text{static}})$ whenever at least two tasks disagree on their best expert.
2. (Noisy routing) If $\sum_t P(t) \varepsilon_t (R_{\text{wrong},t} - R_t(t)) < R_{\text{static}}^* - R_{\text{ideal}}$, where $R_{\text{static}}^* = \inf_{\alpha} R(h_{\text{static}})$, then the MoE still attains lower risk than any static mixture.

The theory above motivates a design that (i) keeps experts specialized and (ii) prevents interference between tasks. Our MINGLE framework achieves both goals by combining

- **Low-rank experts** f_t that capture task-specific variations with minimal parameters, and
- **Null-space constrained gating** that projects gradient updates away from subspaces spanned by previously activated features, keeping ε_t small without harming earlier experts.

3.3 Low-Rank Expert Mixtures for Continual Model Merging

We adopt MoE framework for continual model merging, in which each task i is equipped with a low-rank expert f_i and an associated input-dependent gating function g_i . These components are injected into the linear layers of the backbone (e.g., CLIP visual encoder). The gate g_i modulates expert activation based on the input features, allowing for fine-grained, localized task specialization.

¹Symbols and proofs are deferred to App. A

Mixtures of Low-Rank Expert. When a new task t arrives, a dedicated expert f_t and its gate g_t are appended to the model. The output of a given l -th layer² can be formulated as follows:

$$\theta_t^{\text{merged},(l)}(X) = \theta_{t-1}^{\text{merged},(l)}(X) + g_t^{(l)}(X) \cdot f_t^{(l)}(X) = \theta_0^{(l)}(X) + \sum_{i=1}^t g_i^{(l)}(X) \cdot f_i^{(l)}(X). \quad (2)$$

where only the gate g_t is adaptable during testing, while all experts $\{f_i\}_{i=1}^t$ and old gates $\{g_i\}_{i=1}^{t-1}$ remain frozen to preserve prior knowledge. To construct expert f_t , we first project the task vector $\Delta\theta_t$ onto the orthogonal complement of previously learned directions, following OPCM [68]:

$$\mathcal{P}^{(t-1)}(\Delta\theta_t) = \sum_{p,q=a,p \neq q}^{m,n} \langle \Delta\theta_t, u_p^{(t-1)} v_q^{(t-1)\top} \rangle_F u_p^{(t-1)} v_q^{(t-1)\top}, \quad (3)$$

where $u_p^{(t-1)}$ and $v_q^{(t-1)}$ are the p -th and q -th singular vectors from the singular value decomposition (SVD) of previous experts $\sum_{i=1}^{t-1} f_i(X)$. This projection removes previously learned directions to mitigate interference. We then apply a rank- r truncated SVD for $\mathcal{P}^{(t-1)}(\Delta\theta_t)$ to construct a low-rank expert [20]:

$$f_t = BA = (\tilde{U}\tilde{\Sigma})\tilde{V}^\top, \quad (4)$$

where $\tilde{U} \in \mathbb{R}^{d_1 \times r}$, $\tilde{\Sigma} \in \mathbb{R}^{r \times r}$, and $\tilde{V} \in \mathbb{R}^{d_2 \times r}$, retaining the top r singular components. The resulting expert captures the principal directions while significantly reducing parameter overhead.

Each gating function is implemented as a linear projection:

$$g_t(X) = W_t^{(g)\top} X + b_t^{(g)}, \quad (5)$$

where $W_t^{(g)} \in \mathbb{R}^{d \times 1}$ and $b_t^{(g)} \in \mathbb{R}$ are *learnable* parameters. The gating function is adapted at test time using a small number of unlabeled test data.

Test-Time Adaptation. Given class text embeddings $T = [T_1, \dots, T_{|C_t|}] \in \mathbb{R}^{|C_t| \times d}$, where each T_i is a prompt (e.g., “a photo of a dog”), the model computes logits via scaled cosine similarity: $p(y | x) = \text{softmax}(z(x))$, $z(x) = \tau \cdot \text{norm}(\phi_{\text{img}}(x)) \cdot \text{norm}(\phi_{\text{text}}(T))^\top$, where ϕ_{img} and ϕ_{text} are the image and text encoders, $\text{norm}(\cdot)$ denotes L_2 -normalization, and τ is a temperature scalar.

To encourage the merged model to retain task-specific behavior, we minimize the Kullback–Leibler divergence between its prediction and that of the corresponding individual fine-tuned model θ_t . We define the adaptation objective as:

$$L_t = \mathbb{E}_{x \sim \mathcal{D}_t^{\text{seed}}} \left[\text{KL} \left(p(x; \theta_t^{\text{merged}}) \parallel p(x; \theta_t) \right) \right]. \quad (6)$$

3.4 Adaptive Null-Space Constrained Gating for Interference Mitigation

When merging models continually, the primary challenge of gating is to integrate new experts without disturbing prior task predictions. Consider two experts f_1, f_2 and their corresponding gates g_1, g_2 . When evaluating on the first task domain X_1 , the interference from g_2 can be quantified as:

$$\xi(g_2) = \|g_1(X_1) \cdot f_1(X_1) + g_2(X_1) \cdot f_2(X_1) - f_1(X_1)\|^2. \quad (7)$$

This measures the deviation introduced by g_2 on the domain where f_1 originally dominates. A desirable gating function should suppress $g_2(X_1)$, ensuring predictions on X_1 remain unaffected. However, as X_1 becomes inaccessible after adaptation, this error becomes unobservable and cannot be minimized directly, resulting in prediction drift and catastrophic forgetting.

Hard Null-Space Projection. After finishing task t we cache l -th layer activations on a seed buffer $\mathcal{D}_t^{\text{seed}}$ and estimate its covariance $C_t^{(l)} = \mathbb{E}[\theta_t^{\text{merged},(l)}(X_t) \theta_t^{\text{merged},(l)}(X_t)^\top] \in \mathbb{R}^{d \times d}$. Truncated SVD yields the top- k dominant subspaces $\tilde{U}_t^{(l)} \in \mathbb{R}^{d \times k}$. Concatenating all previous tasks and orthonormalising: $U_t^{(l)} = \text{orthonorm}[U_{t-1}^{(l)} | \tilde{U}_t^{(l)}] \in \mathbb{R}^{d \times tk}$, the hard projector is $P_t = I - U_t^{(l)} U_t^{(l)\top} \in \mathbb{R}^{d \times d}$. To eliminate interference on task $\leq t-1$, the gate update for task t is $W_t^{(g,l)} \leftarrow W_t^{(g,l)} - \eta P_{t-1}^{(l-1)} \nabla L_t^{(l)}$, which may also removes gradient components that are informative for task t whenever its feature support overlaps $\text{span}(U_{t-1})$.

²The layer index l is omitted hereafter whenever it does not cause ambiguity.

Adaptive Null-Space Relaxation. To restore plasticity, we replace the *all-one* eigenvalues of P_{t-1} with *soft* coefficients learned online.

(i) *Interference statistics.* For each column $u_p^{(l)}$ of $U_{t-1}^{(l)}$ we measure instantaneous alignment:

$$r_p^{(l)} = \|(\nabla L_t)^\top u_p^{(l)}\|_2 / \|\nabla L_t\|_2. \quad (8)$$

We maintain per-direction interference scores $S^{(m,l)} \in \mathbb{R}^k$ (initialized to 0) by applying an exponential moving average at each optimization step m :

$$S^{(m,l)} = \beta S^{(m-1,l)} + (1 - \beta) r^{(l)}, \quad (9)$$

which suppresses stochastic gradient noise while preserving the dominant interference directions.

(ii) *Adaptive shrinkage.* Each direction is attenuated by $\lambda^{(m,l)} = \exp(-\gamma S^{(m,l)})$ ($\gamma > 0$, $\lambda^{(m,l)} \in (0, 1]$). Let $\Lambda_{t-1}^{(m,l)} = \text{diag}(\lambda_1^{(m,l)}, \dots, \lambda_{(t-1)\cdot k}^{(m,l)})$. The *relaxed projector* becomes:

$$\tilde{P}_{t-1}^{(m,l)} = U_{t-1}^{(m,l)} \Lambda_{t-1}^{(m,l)} U_{t-1}^{(m,l)\top}, \quad (10)$$

interpolating smoothly between no protection ($\Lambda = 0$) and the hard null projector ($\Lambda = I$).

(iii) *Update rule.* We finally update:

$$W_t^{(g,l)} \leftarrow W_t^{(g,l)} - \eta \tilde{P}_{t-1}^{(l-1)} \nabla L_t^{(l)}. \quad (11)$$

Relaxing the projector inevitably allows more residual interference than the hard null-space variant, yet empirically the increase is minor and is offset by markedly higher plasticity (Tab. 4), indicating a favorable *stability–plasticity balance*. The overall procedure is outlined in Algo. 1.

4 Experiments

We describe the experimental setup in Sec. 4.1, followed by the main results in Sec. 4.2 and further analysis and ablations in Sec. 4.3. Due to page limitations, detailed results are provided in the Appendix.

4.1 Experimental Setup

Datasets and Models. Following [68], we evaluate our method on a diverse set of image classification tasks using CLIP-ViT models [52] as the backbone. Three task groups comprising 8, 14, and 20 tasks are considered to assess scalability. Specifically, we use ViT-B/32, ViT-B/16, and ViT-L/14 models, each fine-tuned on up to 20 downstream tasks. All resulting model checkpoints are publicly available via FusionBench [65]. To evaluate robustness to task order, we repeat experiments over 10 random permutations using seeds ranging from 42 to 51. To enable comparison with conventional continual learning methods, we adopt the Multi-domain Task-Incremental Learning (MTIL) benchmark [93], where eleven tasks are presented in alphabetical order.

Implementation Details. We insert low-rank experts into the linear layers of the CLIP vision encoder. Two variants are considered: a full setup that modifies all attention and MLP linear layers, and a lightweight alternative applied only to `attn.qkv` and `mlp.fc1`. Unless stated otherwise, we adopt the full configuration. Each expert has rank $r = 64$. The null-space constraint uses a subspace

Algorithm 1 MINGLE Procedure.

Input: pre-trained model θ_0 and fine-tuned models $\{\theta_t\}_{t=1}^T$; seed data $\{\mathcal{D}_t^{\text{seed}}\}_{t=1}^T$; hyperparameters k, β, γ ; learning rate η

Output: Merged model θ_T^{merged}

Init: $\theta_0^{\text{merged}} \leftarrow \theta_0$; $U_0^{(l)} \leftarrow \emptyset$

for task $t = 1$ **to** T **do**

▷ create low-rank experts (Eqs. 3 and 4)

$f_t = \text{SVD}(\underbrace{\mathcal{P}^{(t-1)}(\theta_t - \theta_0)}_{\text{use } \theta_1 - \theta_0 \text{ when } t=1}) = B_t A_t$

▷ add expert & initialize gate (Eq. 5)

$\theta_t^{\text{merged}} = \theta_{t-1}^{\text{merged}} + g_t \cdot f_t$

$\{W_t^{(g)}, b_t^{(g)}, S^{(0)}\} \leftarrow 0$

for $m = 1$ **to total steps** **do**

$X \leftarrow \text{batch}(\mathcal{D}_t^{\text{seed}})$

$\{\nabla_{W_t^{(g)}} L, \nabla_{b_t^{(g)}} L\} \leftarrow \nabla L_t(X, \theta_t^{\text{merged}}, \theta_t)$

if $t > 1$ **then**

 ▷ project gradient onto null-space (Eqs. 8-11)

$S^{(m)} = \beta S^{(m-1)} + (1 - \beta) r$

$\nabla_{W_t^{(g)}} L \leftarrow \tilde{P}_{t-1} \nabla_{W_t^{(g)}} L$

end

$W_t^{(g)} \leftarrow W_t^{(g)} - \eta \nabla_{W_t^{(g)}} L$

$b_t^{(g)} \leftarrow b_t^{(g)} - \eta \nabla_{b_t^{(g)}} L$

end

▷ update dominant subspaces

$U_t \leftarrow \text{orthonorm}[U_{t-1} \mid \tilde{U}_t]$

end

Table 1: Comparative results of continual merging methods, reporting average accuracy (ACC) and backward transfer (BWT) over ten task orders (mean \pm std). Best results are in bold; second-best are underlined. MINGLE* denotes a lightweight variant.

Method	ViT-B/32			ViT-B/16			ViT-L/14		
	8 tasks	14 tasks	20 tasks	8 tasks	14 tasks	20 tasks	8 tasks	14 tasks	20 tasks
PRE-TRAINED	48.1	56.9	55.6	55.4	62.0	59.8	64.9	69.1	65.6
FINE-TUNED	90.4	89.3	89.8	92.4	91.3	91.6	94.3	93.4	93.5
C. FINE-TUNED	79.8	67.4	62.6	82.9	72.2	68.2	90.0	70.9	77.7
ACC (%) \uparrow									
AVERAGE (SWA) [25]	66.3 \pm 0.0	65.4 \pm 0.0	61.1 \pm 0.0	72.3 \pm 0.0	69.7 \pm 0.0	64.8 \pm 0.0	80.0 \pm 0.0	77.5 \pm 0.0	71.1 \pm 0.0
C. TASK ARITHMETIC [23]	67.5 \pm 0.0	66.5 \pm 0.0	60.0 \pm 0.0	77.1 \pm 0.0	70.9 \pm 0.6	64.2 \pm 0.0	82.1 \pm 0.0	77.9 \pm 0.0	70.3 \pm 0.0
C. TIES-MERGING [82]	49.0 \pm 10.2	66.2 \pm 0.6	59.9 \pm 0.7	66.8 \pm 3.7	70.5 \pm 0.8	63.0 \pm 1.6	64.3 \pm 7.0	78.0 \pm 0.6	68.3 \pm 0.9
MAGMAX-IND [39]	70.7 \pm 0.0	67.0 \pm 0.0	61.2 \pm 0.0	76.7 \pm 1.8	67.0 \pm 0.0	62.5 \pm 0.0	83.4 \pm 0.0	71.2 \pm 0.0	71.2 \pm 0.0
OPCM [68]	75.5 \pm 0.5	71.9 \pm 0.3	65.7 \pm 0.2	81.8 \pm 0.3	77.1 \pm 0.5	70.3 \pm 0.2	87.0 \pm 0.4	83.5 \pm 0.2	76.0 \pm 0.2
MINGLE	85.8 \pm 0.8	81.6 \pm 1.4	77.1 \pm 2.0	88.3 \pm 0.6	84.9 \pm 0.8	81.9 \pm 0.9	-	-	-
MINGLE*	<u>85.0</u> \pm 0.5	<u>81.7</u> \pm 1.0	<u>77.1</u> \pm 1.3	<u>87.0</u> \pm 0.6	<u>84.7</u> \pm 1.0	<u>81.6</u> \pm 1.3	91.4 \pm 0.3	89.2 \pm 0.1	83.6 \pm 0.6
BWT (%) \uparrow									
AVERAGE (SWA) [25]	-11.5 \pm 2.2	-8.0 \pm 1.3	-7.1 \pm 2.1	-9.7 \pm 1.5	-7.1 \pm 1.4	-7.3 \pm 1.7	-7.3 \pm 1.4	-5.8 \pm 1.0	-6.4 \pm 1.5
C. TASK ARITHMETIC [23]	-9.6 \pm 1.5	-1.3 \pm 1.6	-3.4 \pm 1.0	-4.2 \pm 1.0	-1.3 \pm 0.4	-3.6 \pm 0.4	-7.1 \pm 0.8	-1.8 \pm 0.3	-3.3 \pm 0.3
C. TIES-MERGING [82]	-15.3 \pm 8.0	1.9 \pm 0.6	-1.5 \pm 0.7	-5.5 \pm 0.4	1.4 \pm 0.7	-1.5 \pm 1.2	-13.0 \pm 5.7	-1.1 \pm 0.4	-2.9 \pm 1.0
MAGMAX-IND [39]	-8.3 \pm 1.3	-7.4 \pm 1.4	-7.2 \pm 1.6	-6.1 \pm 1.3	-7.4 \pm 2.0	-8.0 \pm 2.2	-5.0 \pm 0.8	-6.0 \pm 2.1	-6.5 \pm 2.1
OPCM [68]	-6.3 \pm 1.1	-6.0 \pm 1.0	-7.8 \pm 1.5	-4.8 \pm 0.7	-5.1 \pm 1.4	-6.3 \pm 2.2	-2.6 \pm 1.0	-4.3 \pm 0.7	-6.5 \pm 1.8
MINGLE	-0.6 \pm 0.4	-1.1 \pm 0.3	-2.2 \pm 0.8	-0.4 \pm 0.1	-0.9 \pm 0.1	-1.9 \pm 0.4	-	-	-
MINGLE*	-0.1 \pm 0.1	-0.4 \pm 0.1	-1.3 \pm 0.6	-0.1 \pm 0.1	-0.3 \pm 0.1	-1.0 \pm 0.4	-0.2 \pm 0.0	-0.4 \pm 0.2	-1.5 \pm 0.6

Table 2: Robustness results for ViT-B/32 continual merged on four tasks.

Method	Clean	Motion	Impulse	Gaussian	Pixelate	Spatter	Contrast	JPEG	Avg.
ACC (%) \uparrow									
C. LAYER-WISE ADAMERGING [83]	56.0 \pm 5.3	47.5 \pm 4.4	43.1 \pm 2.3	43.3 \pm 3.4	18.1 \pm 4.7	46.6 \pm 3.0	48.9 \pm 4.8	49.1 \pm 4.0	44.9
C. WEMOE [66]	3.4 \pm 0.8	3.1 \pm 0.4	4.3 \pm 1.4	3.4 \pm 1.4	3.0 \pm 1.6	4.0 \pm 0.9	3.3 \pm 0.7	4.0 \pm 1.2	3.6
C. TASK ARITHMETIC [23]	77.5 \pm 0.0	66.0 \pm 0.0	58.9 \pm 0.0	59.6 \pm 0.0	29.7 \pm 0.0	63.5 \pm 0.0	66.0 \pm 0.0	67.8 \pm 0.0	61.1
MAGMAX-IND [39]	79.1 \pm 0.0	69.0 \pm 0.0	60.6 \pm 0.0	61.5 \pm 0.0	33.0 \pm 0.0	66.4 \pm 0.0	68.6 \pm 0.0	69.9 \pm 0.0	63.5
OPCM [68]	83.6 \pm 0.5	72.5 \pm 0.6	64.7 \pm 1.2	65.2 \pm 1.2	35.2 \pm 0.6	70.5 \pm 0.5	72.5 \pm 0.6	74.4 \pm 0.3	67.3
MINGLE	89.9 \pm 0.4	82.8 \pm 0.8	67.5 \pm 2.0	70.7 \pm 1.2	37.9 \pm 0.4	77.0 \pm 0.7	80.1 \pm 0.8	82.9 \pm 0.9	73.2
BWT (%) \uparrow									
C. LAYER-WISE ADAMERGING [83]	-38.0 \pm 7.1	-37.3 \pm 5.9	-22.2 \pm 3.0	-25.2 \pm 4.5	-20.8 \pm 6.3	-28.6 \pm 4.0	-34.7 \pm 6.5	-36.1 \pm 5.3	-29.5
C. WEMOE [66]	-30.7 \pm 3.1	-28.7 \pm 3.8	-22.1 \pm 11.6	-25.5 \pm 9.8	-8.0 \pm 4.5	-23.4 \pm 11.0	-27.6 \pm 5.6	-28.6 \pm 5.2	-24.3
C. TASK ARITHMETIC [23]	-4.8 \pm 0.9	-6.1 \pm 1.2	-1.6 \pm 3.0	-1.6 \pm 1.7	-2.7 \pm 1.5	-3.1 \pm 2.5	-6.1 \pm 1.2	-5.1 \pm 0.8	-3.9
MAGMAX-IND [39]	-7.7 \pm 0.8	-8.1 \pm 1.5	-6.1 \pm 4.9	-5.1 \pm 3.7	-3.5 \pm 3.0	-7.3 \pm 2.9	-8.4 \pm 1.6	-8.2 \pm 1.2	-6.8
OPCM [68]	-4.3 \pm 1.8	-4.5 \pm 2.8	-6.4 \pm 7.1	-6.1 \pm 4.3	-2.9 \pm 0.9	-6.3 \pm 2.9	-4.5 \pm 2.8	-5.7 \pm 1.5	-5.1
MINGLE	-0.2 \pm 0.2	-0.1 \pm 0.4	0.7 \pm 1.0	0.6 \pm 1.1	-0.2 \pm 1.1	0.2 \pm 0.7	0.0 \pm 0.5	0.5 \pm 0.5	-0.2

dimension $k = 3$, with relaxation coefficients $\gamma = 1$ and $\beta = 0.99$. For each task, the merged model is adapted over 50 iterations using the Adam optimizer with a learning rate of $1e-4$ and a batch size of 16. We draw 5 unlabeled test data per class, with no access to data from previous tasks.

Evaluation Metrics. We evaluate performance using average accuracy (ACC) and backward transfer (BWT) [36]. ACC measures the mean accuracy over all tasks using the final merged model: $ACC = \frac{1}{T} \sum_{i=1}^T a_i(\theta_t^{\text{merged}})$, where $a_i(\cdot)$ denotes the accuracy on task i . BWT quantifies the extent of forgetting by comparing performance on earlier tasks before and after merging: $BWT = \frac{1}{T-1} \sum_{i=1}^{T-1} [a_i(\theta_t^{\text{merged}}) - a_i(\theta_i^{\text{merged}})]$.

4.2 Main Results

Overall Performance As shown in Tab. 1, MINGLE substantially outperforms existing continual merging approaches across all CLIP backbones and task counts, achieving the highest accuracy while nearly eliminating backward forgetting. These results confirm that our method consistently delivers both strong task accuracy and long-term stability under diverse continual scenarios.

Robustness to Test-Time Distribution Shifts. Following prior work [83, 66], we evaluate MINGLE on seven corruptions (motion blur, impulse noise, Gaussian noise, pixelate, spatter, contrast, JPEG) and report results in Tab. 2. It preserves high accuracy and near-zero or even positive BWT,

Table 3: Comparison of last accuracy (%) with conventional CL approaches on MTIL benchmark.

Method	Aircraft	Caltech101	CIFAR100	DTD	EuroSAT	Flowers	Food101	MNIST	Pets	Cars	SUN397	Avg.
Conventional CL (Sequential fine-tuned)												
WISE-FT [77]	27.2	90.8	68.0	68.9	86.9	74.0	87.6	99.6	92.6	77.8	<u>81.3</u>	77.7
ZSCL [93]	40.6	92.2	81.3	70.5	94.8	90.5	91.9	98.7	93.9	85.3	80.2	83.6
MoE-ADAPTER [85]	49.8	92.2	86.1	78.1	95.7	94.3	89.5	98.1	89.9	81.6	80.0	85.0
DIKI [69]	45.2	95.7	<u>86.3</u>	72.9	98.0	<u>97.0</u>	89.2	<u>99.4</u>	94.2	81.6	76.6	85.1
AWOFORGET [92]	42.4	92.7	83.2	73.2	97.0	91.8	92.2	99.1	<u>93.9</u>	87.4	82.6	85.0
DUAL-RAIL [81]	<u>52.5</u>	96.8	83.3	80.1	96.4	99.0	89.9	98.8	93.5	<u>85.5</u>	79.2	86.8
MAGMAX [39]	40.2	96.1	81.1	72.0	<u>97.8</u>	76.3	88.4	99.2	93.0	70.5	68.9	80.3
MINGLE-SEQ	58.7	97.5	87.2	<u>79.7</u>	97.3	87.2	90.1	99.6	93.0	80.4	73.3	<u>85.8</u>
Continual Merging (Independent fine-tuned)												
AVERAGE (SWA) [25]	26.5	92.3	74.3	48.4	73.7	74.0	87.1	84.0	91.2	67.5	68.5	71.6
C. TA [23]	26.6	92.5	74.5	48.7	74.3	74.4	87.0	85.5	91.2	67.7	68.6	71.9
C. TIES [82]	30.5	94.0	74.8	49.8	71.7	73.8	<u>87.3</u>	81.5	90.6	67.0	67.9	71.7
MAGMAX-IND [39]	29.9	93.7	<u>78.4</u>	46.1	58.3	68.1	86.8	82.8	91.4	62.7	69.3	69.8
OPCM [68]	<u>35.7</u>	<u>95.9</u>	77.0	<u>54.6</u>	<u>90.3</u>	<u>76.4</u>	87.1	<u>96.3</u>	<u>93.3</u>	<u>70.1</u>	<u>70.5</u>	<u>77.0</u>
MINGLE	54.2	97.3	79.7	72.3	96.0	86.7	88.7	99.3	93.9	73.1	71.6	83.0

Table 4: Ablation study of MINGLE with CLIP ViT-B/16 over 8, 14, and 20 tasks.

Test-Time	Frozen	Null-Space	Adaptive	ACC(%) ↑			BWT(%) ↑		
Adaptation	Old Gate	Constrained Gate	Relaxation	8 tasks	14 tasks	20 tasks	8 tasks	14 tasks	20 tasks
✗	—	—	—	78.7 ±0.1	76.4 ±1.0	70.6 ±0.4	-0.5 ±0.1	-1.0 ±0.3	-1.3 ±0.3
✓	✗	✗	✗	86.4 ±5.3	81.7 ±2.3	76.7 ±1.3	-6.0 ±5.2	-7.7 ±3.4	-12.8 ±1.3
✓	✓	✗	✗	87.4 ±0.4	81.3 ±0.8	76.2 ±1.3	-2.3 ±0.5	-4.3 ±0.8	-6.8 ±0.9
✓	✓	✓	✗	86.0 ±1.5	83.5 ±0.9	78.3 ±1.7	-0.1 ±0.1	-0.1 ±0.1	-0.2 ±0.1
✓	✓	✓	✓	88.3 ±0.6	84.9 ±0.8	81.9 ±0.9	-0.4 ±0.1	-0.9 ±0.1	-1.9 ±0.4

outperforming all baselines, whereas direct application of SOTA TTA-based merging (WEMOE, AdaMerging) in a continual setting fails without tailored designs to continual setup.

Comparison with Conventional CL. Tab. 3 evaluates two CL paradigms on the MTIL benchmark: conventional CL, where each task model is fine-tuned from its immediate predecessor; and continual merging, which fine-tunes each task model independently before fusion, eliminating inter-model dependencies and enabling flexible task ordering and model reuse. Within the merging family, MINGLE sets a new state-of-the-art, and when integrated into a sequential fine-tuning pipeline, it matches the performance of SOTA CL methods. This demonstrates both its strength as a fusion strategy and its versatility across different training regimes.

4.3 Ablation Results and Analysis

Ablation Study. We explore the contribution of each component in Tab. 4. Row 1 shows a fixed-weight merging of low-rank experts as our baseline. In Row 2, adding TTA boosts ACC substantially but at the cost of worsening BWT with more tasks. Row 3 demonstrates that freezing earlier gates curbs forgetting while retaining ACC gains. Row 4 then applies null-space constraints, yielding further BWT improvements. Finally, Row 5 presents the full method with adaptive relaxation, which best harmonizes accuracy and long-term stability.

Computation and Parameter Efficiency. Tab. 5 compares different expert insertion layers and rank settings for CLIP-ViT-B/32 on eight tasks. Embedding experts in both `attn` and `mlp` layers achieves the highest accuracy at the cost of increased TTA time and parameter overhead. A hybrid scheme (`qkv & fc1`, $r = 64$) delivers a favorable balance. In the rank sweep, moving from $r = 32$ to 64 yields a clear ACC gain, while further increasing r leads to diminishing or negative returns. Experiments were run on a single RTX 4090 GPU. These results highlight MINGLE’s flexibility under diverse resource budgets.

Table 5: Efficiency analysis on TTA time, trainable/full parameter count, and accuracy for CLIP-ViT-B/32 merged on eight tasks.

Configuration	Time	T. Param	F. Param	ACC
<code>attn & mlp</code> ($r = 64$)	78 s	83.0 K	173.1 M	85.8
<code>attn.qkv_proj</code> ($r = 64$)	61 s	27.7 K	116.0 M	69.9
<code>attn.out_proj</code> ($r = 64$)	47 s	9.3 K	97.0 M	53.9
<code>mlp.fc1</code> ($r = 64$)	48 s	9.0 K	111.1 M	82.6
<code>mlp.fc2</code> ($r = 64$)	48 s	36.8 K	111.3 M	70.1
<code>qkv & fc1</code> ($r = 32$)	65 s	36.9 K	113.7 M	84.5
<code>qkv & fc1</code> ($r = 64$)	65 s	36.9 K	139.7 M	85.0
<code>qkv & fc1</code> ($r = 128$)	65 s	36.9 K	191.6 M	85.1
<code>qkv & fc1</code> ($r = 768$)	70 s	36.9 K	710.3 M	83.7

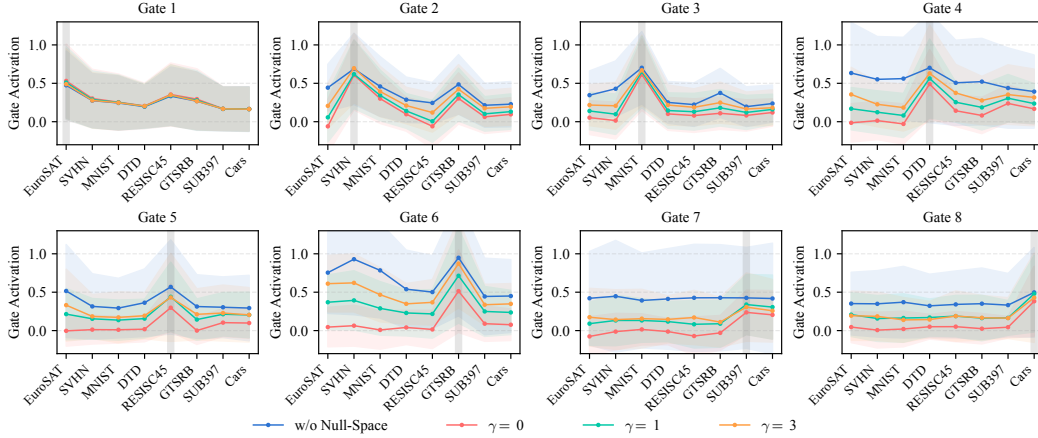


Figure 3: Gate activations across eight tasks under varying γ . Each subplot shows one gate; curves and shaded areas indicate mean and std across layers. Gray bars mark the gate’s training task. Lower γ leads to stronger suppression on prior tasks.

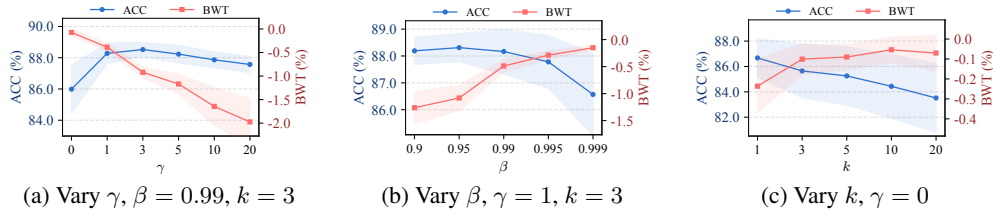


Figure 4: Sensitivity analysis of the null-space constrained gating *w.r.t.* hyper-parameters β , γ , and k .

Number of Seed Samples The quantity of seed samples plays a central role in determining the reliability and efficiency of TTA. We examine how varying the number of seed samples per class impacts performance with CLIP ViT-B/16. As shown in Fig. 5, even a single sample per class yields strong results, with only minor gains from additional samples. This indicates that TTA is largely robust to sample quantity. We also observe reduced variance across task orders as more samples are used, motivating our choice of five samples per class as a balanced trade-off between performance and efficiency.

Hyper-parameter of Gate. We study the effect of three key hyper-parameters: γ , β , and k . γ controls the strength of null-space suppression; smaller values lead to stronger attenuation of activations on prior tasks, reducing forgetting (Fig. 3, 4a). As shown in Fig. 4b, β regulates the smoothness of the EMA used to accumulate interference signals. A moderate setting ($\beta = 0.99$) balances responsiveness and stability. Smaller β amplifies noise sensitivity, while larger β slows detection of interference. k determines the number of principal directions retained per task; performance saturates at $k = 3$ (Fig. 4c), indicating that a small number of task-specific directions suffices.

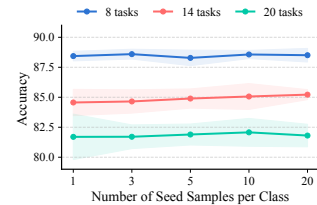


Figure 5: Analysis of seed sample quantity on performance.

5 Conclusions

We proposed MINGLE, a test-time continual model merging (TTCMM) approach that integrates test-time adaptation into continual model merging via a mixture-of-experts architecture and Adaptive Null-Space Constrained Gating. Extensive empirical evaluations confirmed that MINGLE significantly improves generalization performance and mitigates catastrophic forgetting, consistently surpassing previous state-of-the-art methods. These results highlight MINGLE’s capability to efficiently adapt to new tasks without revisiting original training data, demonstrating the practical advantages of our proposed TTCMM framework in realistic continual learning applications.

References

- [1] S. K. Ainsworth, J. Hayase, and S. Srinivasa. Git re-basin: Merging models modulo permutation symmetries. *arXiv preprint arXiv:2209.04836*, 2022.
- [2] R. Aljundi, F. Babiloni, M. Elhoseiny, M. Rohrbach, and T. Tuytelaars. Memory aware synapses: Learning what (not) to forget. In *Proceedings of the European conference on computer vision (ECCV)*, pages 139–154, 2018.
- [3] L. Bossard, M. Guillaumin, and L. Van Gool. Food-101—mining discriminative components with random forests. In *European Conference on Computer Vision*, pages 446–461. Springer, 2014.
- [4] G. Cheng, J. Han, and X. Lu. Remote sensing image scene classification: Benchmark and state of the art. *Proceedings of the IEEE*, 105(10):1865–1883, 2017.
- [5] R. Chitale, A. Vaidya, A. Kane, and A. S. Ghotkar. Task arithmetic with loRA for continual learning. In *Workshop on Advancing Neural Network Training: Computational Efficiency, Scalability, and Resource Optimization (WANT@NeurIPS 2023)*, 2023.
- [6] M. Cimpoi, S. Maji, I. Kokkinos, S. Mohamed, and A. Vedaldi. Describing textures in the wild. In *Proceedings of the IEEE Conference on Computer Vision and Pattern Recognition*, pages 3606–3613, 2014.
- [7] T. Clanuwat, M. Bober-Irizar, A. Kitamoto, A. Lamb, K. Yamamoto, and D. Ha. Deep learning for classical japanese literature. In *NeurIPS Workshop on Machine Learning for Creativity and Design*, 2018.
- [8] A. Coates, A. Y. Ng, and H. Lee. An analysis of single-layer networks in unsupervised feature learning. In *Proceedings of the Fourteenth International Conference on Artificial Intelligence and Statistics*, pages 215–223. JMLR Workshop and Conference Proceedings, 2011.
- [9] G. Cohen, S. Afshar, J. Tapson, and A. Van Schaik. Emnist: Extending mnist to handwritten letters. In *2017 International Joint Conference on Neural Networks (IJCNN)*, pages 2921–2926. IEEE, 2017.
- [10] M. Döbler, R. A. Marsden, and B. Yang. Robust mean teacher for continual and gradual test-time adaptation. In *Proceedings of the IEEE/CVF Conference on Computer Vision and Pattern Recognition*, pages 7704–7714, 2023.
- [11] A. Douillard, M. Cord, C. Ollion, T. Robert, and E. Valle. Podnet: Pooled outputs distillation for small-tasks incremental learning. *European Conference on Computer Vision*, 2020.
- [12] R. Entezari, H. Sedghi, O. Saukh, and B. Neyshabur. The role of permutation invariance in linear mode connectivity of neural networks. *arXiv preprint arXiv:2110.06296*, 2021.
- [13] C. Fang, A. Dziedzic, L. Zhang, L. Oliva, A. Verma, F. Razak, N. Papernot, and B. Wang. Decentralised, collaborative, and privacy-preserving machine learning for multi-hospital data. *EBioMedicine*, 101, 2024.
- [14] C.-M. Feng, K. Yu, Y. Liu, S. Khan, and W. Zuo. Diverse data augmentation with diffusions for effective test-time prompt tuning. In *Proceedings of the IEEE/CVF International Conference on Computer Vision*, pages 2704–2714, 2023.
- [15] T. Fukuda, H. Kera, and K. Kawamoto. Adapter merging with centroid prototype mapping for scalable class-incremental learning. *arXiv preprint arXiv:2412.18219*, 2024.
- [16] J. Gao, J. Zhang, X. Liu, T. Darrell, E. Shelhamer, and D. Wang. Back to the source: Diffusion-driven adaptation to test-time corruption. In *Proceedings of the IEEE/CVF Conference on Computer Vision and Pattern Recognition*, pages 11786–11796, 2023.
- [17] I. J. Goodfellow, D. Erhan, P.-L. Carrier, A. Courville, M. Mirza, B. Hamner, W. Cukierski, Y. Tang, D. Thaler, D.-H. Lee, et al. Challenges in representation learning: A report on three machine learning contests. In *International Conference on Neural Information Processing*, pages 117–124. Springer, 2013.

- [18] P. Helber, B. Bischke, A. Dengel, and D. Borth. Eurosat: A novel dataset and deep learning benchmark for land use and land cover classification. *IEEE Journal of Selected Topics in Applied Earth Observations and Remote Sensing*, 12(7):2217–2226, 2019.
- [19] S. Hou, X. Pan, C. C. Loy, Z. Wang, and D. Lin. Learning a unified classifier incrementally via rebalancing. *2019 IEEE/CVF Conference on Computer Vision and Pattern Recognition (CVPR)*, pages 831–839, 2019.
- [20] E. J. Hu, Y. Shen, P. Wallis, Z. Allen-Zhu, Y. Li, S. Wang, L. Wang, W. Chen, et al. Lora: Low-rank adaptation of large language models. *ICLR*, 1(2):3, 2022.
- [21] C. Huang, Q. Liu, B. Y. Lin, T. Pang, C. Du, and M. Lin. Lorahub: Efficient cross-task generalization via dynamic loRA composition. In *First Conference on Language Modeling*, 2024.
- [22] L. Huang, X. Cao, H. Lu, and X. Liu. Class-incremental learning with clip: Adaptive representation adjustment and parameter fusion. In *European Conference on Computer Vision*, pages 214–231. Springer, 2024.
- [23] G. Ilharco, M. T. Ribeiro, M. Wortsman, L. Schmidt, H. Hajishirzi, and A. Farhadi. Editing models with task arithmetic. In *The Eleventh International Conference on Learning Representations*, 2023.
- [24] Y. Iwasawa and Y. Matsuo. Test-time classifier adjustment module for model-agnostic domain generalization. *Advances in Neural Information Processing Systems*, 34:2427–2440, 2021.
- [25] P. Izmailov, D. Podoprikin, T. Garipov, D. Vetrov, and A. G. Wilson. Averaging weights leads to wider optima and better generalization. In *34th Conference on Uncertainty in Artificial Intelligence 2018, UAI 2018*, pages 876–885. Association For Uncertainty in Artificial Intelligence (AUAI), 2018.
- [26] R. A. Jacobs, M. I. Jordan, S. J. Nowlan, and G. E. Hinton. Adaptive mixtures of local experts. *Neural computation*, 3(1):79–87, 1991.
- [27] X. Jin, X. Ren, D. Preotiuc-Pietro, and P. Cheng. Dataless knowledge fusion by merging weights of language models. *arXiv preprint arXiv:2212.09849*, 2022.
- [28] M. I. Jordan and R. A. Jacobs. Hierarchical mixtures of experts and the em algorithm. *Neural computation*, 6(2):181–214, 1994.
- [29] S. Jung, H. Ahn, S. Cha, and T. Moon. Continual learning with node-importance based adaptive group sparse regularization. *Advances in neural information processing systems*, 33:3647–3658, 2020.
- [30] J. Kirkpatrick, R. Pascanu, N. C. Rabinowitz, J. Veness, G. Desjardins, A. A. Rusu, K. Milan, J. Quan, T. Ramalho, A. Grabska-Barwinska, D. Hassabis, C. Clopath, D. Kumaran, and R. Hadsell. Overcoming catastrophic forgetting in neural networks. *Proceedings of the National Academy of Sciences*, 114:3521 – 3526, 2016.
- [31] J. Krause, M. Stark, J. Deng, and L. Fei-Fei. 3d object representations for fine-grained categorization. In *2013 IEEE International Conference on Computer Vision Workshops*, pages 554–561. IEEE, 2013.
- [32] A. Krizhevsky and G. Hinton. Learning multiple layers of features from tiny images. Technical report, University of Toronto, 2009.
- [33] Y. LeCun, L. Bottou, Y. Bengio, and P. Haffner. Gradient-based learning applied to document recognition. *Proceedings of the IEEE*, 86(11):2278–2324, 1998.
- [34] S.-W. Lee, J.-H. Kim, J. Jun, J.-W. Ha, and B.-T. Zhang. Overcoming catastrophic forgetting by incremental moment matching. *Advances in neural information processing systems*, 30, 2017.
- [35] Y. Lee, D. Kim, J. Kang, J. Bang, H. Song, and J.-G. Lee. RA-TTA: Retrieval-augmented test-time adaptation for vision-language models. In *The Thirteenth International Conference on Learning Representations*, 2025.

- [36] S. Lin, L. Yang, D. Fan, and J. Zhang. Beyond not-forgetting: Continual learning with backward knowledge transfer. *Advances in Neural Information Processing Systems*, 35:16165–16177, 2022.
- [37] T. Y. Liu and S. Soatto. Tangent model composition for ensembling and continual fine-tuning. In *Proceedings of the IEEE/CVF International Conference on Computer Vision*, pages 18676–18686, 2023.
- [38] Y. Liu, B. Schiele, and Q. Sun. Rmm: Reinforced memory management for class-incremental learning. *Advances in Neural Information Processing Systems*, 34:3478–3490, 2021.
- [39] D. Marczak, B. Twardowski, T. Trzcinski, and S. Cygert. Magmax: Leveraging model merging for seamless continual learning. In *European Conference on Computer Vision (ECCV)*, 2024.
- [40] I. E. Marouf, S. Roy, E. Tartaglione, and S. Lathuilière. Weighted ensemble models are strong continual learners, 2024.
- [41] M. McCloskey and N. J. Cohen. Catastrophic interference in connectionist networks: The sequential learning problem. In *Psychology of learning and motivation*, volume 24, pages 109–165. Elsevier, 1989.
- [42] B. McMahan, E. Moore, D. Ramage, S. Hampson, and B. A. y Arcas. Communication-efficient learning of deep networks from decentralized data. In *Artificial intelligence and statistics*, pages 1273–1282. PMLR, 2017.
- [43] S. Mu and S. Lin. A comprehensive survey of mixture-of-experts: Algorithms, theory, and applications. *arXiv preprint arXiv:2503.07137*, 2025.
- [44] Y. Netzer, T. Wang, A. Coates, A. Bissacco, B. Wu, and A. Y. Ng. Reading digits in natural images with unsupervised feature learning. In *NIPS Workshop on Deep Learning and Unsupervised Feature Learning*, 2011.
- [45] M.-E. Nilsback and A. Zisserman. Automated flower classification over a large number of classes. In *2008 Sixth Indian Conference on Computer Vision, Graphics & Image Processing*, pages 722–729. IEEE, 2008.
- [46] S. Niu, J. Wu, Y. Zhang, Y. Chen, S. Zheng, P. Zhao, and M. Tan. Efficient test-time model adaptation without forgetting. In *International conference on machine learning*, pages 16888–16905. PMLR, 2022.
- [47] G. Ortiz-Jimenez, A. Favero, and P. Frossard. Task arithmetic in the tangent space: Improved editing of pre-trained models. *Advances in Neural Information Processing Systems*, 36:66727–66754, 2023.
- [48] O. M. Parkhi, A. Vedaldi, A. Zisserman, and C. V. Jawahar. Cats and dogs. *2012 IEEE Conference on Computer Vision and Pattern Recognition*, pages 3498–3505, 2012.
- [49] A. Porrello, L. Bonicelli, P. Buzzega, M. Millunzi, S. Calderara, and R. Cucchiara. A second-order perspective on model compositionality and incremental learning. In *The Thirteenth International Conference on Learning Representations*, 2025.
- [50] Z. Qiu, L. Xu, Z. Wang, Q. Wu, F. Meng, and H. Li. Ism-net: Mining incremental semantics for class incremental learning. *Neurocomputing*, 523:130–143, 2023.
- [51] Z. Qiu, Y. Xu, F. Meng, H. Li, L. Xu, and Q. Wu. Dual-consistency model inversion for non-exemplar class incremental learning. In *Proceedings of the IEEE/CVF conference on computer vision and pattern recognition*, pages 24025–24035, 2024.
- [52] A. Radford, J. W. Kim, C. Hallacy, A. Ramesh, G. Goh, S. Agarwal, G. Sastry, A. Askell, P. Mishkin, J. Clark, et al. Learning transferable visual models from natural language supervision. In *International conference on machine learning*, pages 8748–8763. PmLR, 2021.
- [53] S.-A. Rebuffi, A. Kolesnikov, G. Sperl, and C. H. Lampert. icarl: Incremental classifier and representation learning. *2017 IEEE Conference on Computer Vision and Pattern Recognition (CVPR)*, pages 5533–5542, 2016.

- [54] S. Schneider, E. Rusak, L. Eck, O. Bringmann, W. Brendel, and M. Bethge. Improving robustness against common corruptions by covariate shift adaptation. *Advances in neural information processing systems*, 33:11539–11551, 2020.
- [55] Y. Shen, K. Song, X. Tan, D. Li, W. Lu, and Y. Zhuang. Hugginggpt: Solving ai tasks with chatgpt and its friends in hugging face. *Advances in Neural Information Processing Systems*, 36:38154–38180, 2023.
- [56] K. Shoemake. Animating rotation with quaternion curves. In *Proceedings of the 12th annual conference on Computer graphics and interactive techniques*, pages 245–254, 1985.
- [57] M. Shu, W. Nie, D.-A. Huang, Z. Yu, T. Goldstein, A. Anandkumar, and C. Xiao. Test-time prompt tuning for zero-shot generalization in vision-language models. *Advances in Neural Information Processing Systems*, 35:14274–14289, 2022.
- [58] C. Simon, P. Koniusz, and M. Harandi. On learning the geodesic path for incremental learning. In *Proceedings of the IEEE/CVF conference on Computer Vision and Pattern Recognition*, pages 1591–1600, 2021.
- [59] J. S. Smith, L. Karlinsky, V. Gutta, P. Cascante-Bonilla, D. Kim, A. Arbelle, R. Panda, R. Feris, and Z. Kira. Coda-prompt: Continual decomposed attention-based prompting for rehearsal-free continual learning. In *Proceedings of the IEEE/CVF Conference on Computer Vision and Pattern Recognition*, pages 11909–11919, 2023.
- [60] R. Socher, A. Perelygin, J. Wu, J. Chuang, C. D. Manning, A. Ng, and C. Potts. Recursive deep models for semantic compositionality over a sentiment treebank. In *Proceedings of the 2013 Conference on Empirical Methods in Natural Language Processing*, pages 1631–1642, 2013.
- [61] J. Song, J. Lee, I. S. Kweon, and S. Choi. Ecotta: Memory-efficient continual test-time adaptation via self-distilled regularization. In *Proceedings of the IEEE/CVF Conference on Computer Vision and Pattern Recognition*, pages 11920–11929, 2023.
- [62] J. Stallkamp, M. Schlipsing, J. Salmen, and C. Igel. Man vs. computer: Benchmarking machine learning algorithms for traffic sign recognition. *Neural Networks*, 32:323–332, 2012.
- [63] G. Stoica, P. Ramesh, B. Ecsedi, L. Choshen, and J. Hoffman. Model merging with SVD to tie the knots. In *The Thirteenth International Conference on Learning Representations*, 2025.
- [64] Y. Sun, X. Wang, Z. Liu, J. Miller, A. Efros, and M. Hardt. Test-time training with self-supervision for generalization under distribution shifts. In *International conference on machine learning*, pages 9229–9248. PMLR, 2020.
- [65] A. Tang, L. Shen, Y. Luo, H. Hu, B. Du, and D. Tao. FusionBench: A Comprehensive Benchmark of Deep Model Fusion, June 2024.
- [66] A. Tang, L. Shen, Y. Luo, N. Yin, L. Zhang, and D. Tao. Merging multi-task models via weight-ensembling mixture of experts. In *International Conference on Machine Learning*, pages 47778–47799. PMLR, 2024.
- [67] A. Tang, L. Shen, Y. Luo, Y. Zhan, H. Hu, B. Du, Y. Chen, and D. Tao. Parameter-efficient multi-task model fusion with partial linearization. In *The Twelfth International Conference on Learning Representations*, 2024.
- [68] A. Tang, E. Yang, L. Shen, Y. Luo, H. Hu, B. Du, and D. Tao. Merging models on the fly without retraining: A sequential approach to scalable continual model merging. *arXiv preprint arXiv:2501.09522*, 2025.
- [69] L. Tang, Z. Tian, K. Li, C. He, H. Zhou, H. Zhao, X. Li, and J. Jia. Mind the interference: Retaining pre-trained knowledge in parameter efficient continual learning of vision-language models. In *European Conference on Computer Vision*, pages 346–365. Springer, 2024.
- [70] J. Utans. Weight averaging for neural networks and local resampling schemes. In *Proc. AAAI-96 Workshop on Integrating Multiple Learned Models*. AAAI Press, pages 133–138. Citeseer, 1996.

- [71] B. S. Veeling, J. Linmans, J. Winkens, T. S. Cohen, and M. Welling. Rotation equivariant cnns for digital pathology. *arXiv preprint arXiv:1806.03962*, 2018.
- [72] D. Wang, E. Shelhamer, S. Liu, B. Olshausen, and T. Darrell. Tent: Fully test-time adaptation by entropy minimization. *arXiv preprint arXiv:2006.10726*, 2020.
- [73] H. Wang, B. Ping, S. Wang, X. Han, Y. Chen, Z. Liu, and M. Sun. Lora-flow: Dynamic lora fusion for large language models in generative tasks. In *Proceedings of the 62nd Annual Meeting of the Association for Computational Linguistics (Volume 1: Long Papers)*, pages 12871–12882, 2024.
- [74] X. Wang, T. Chen, Q. Ge, H. Xia, R. Bao, R. Zheng, Q. Zhang, T. Gui, and X. Huang. Orthogonal subspace learning for language model continual learning. In *The 2023 Conference on Empirical Methods in Natural Language Processing*, 2023.
- [75] Z. Wang, Z. Zhang, S. Ebrahimi, R. Sun, H. Zhang, C.-Y. Lee, X. Ren, G. Su, V. Perot, J. Dy, et al. Dualprompt: Complementary prompting for rehearsal-free continual learning. In *European Conference on Computer Vision*, pages 631–648. Springer, 2022.
- [76] Z. Wang, Z. Zhang, C.-Y. Lee, H. Zhang, R. Sun, X. Ren, G. Su, V. Perot, J. Dy, and T. Pfister. Learning to prompt for continual learning. In *Proceedings of the IEEE/CVF conference on computer vision and pattern recognition*, pages 139–149, 2022.
- [77] M. Wortsman, G. Ilharco, J. W. Kim, M. Li, S. Kornblith, R. Roelofs, R. G. Lopes, H. Hajishirzi, A. Farhadi, H. Namkoong, et al. Robust fine-tuning of zero-shot models. In *Proceedings of the IEEE/CVF conference on computer vision and pattern recognition*, pages 7959–7971, 2022.
- [78] Y. Wu, L.-K. Huang, R. Wang, D. Meng, and Y. Wei. Meta continual learning revisited: Implicitly enhancing online hessian approximation via variance reduction. In *The Twelfth International Conference on Learning Representations*, 2024.
- [79] H. Xiao, K. Rasul, and R. Vollgraf. Fashion-mnist: a novel image dataset for benchmarking machine learning algorithms. *arXiv preprint arXiv:1708.07747*, 2017.
- [80] J. Xiao, J. Hays, K. A. Ehinger, A. Oliva, and A. Torralba. Sun database: Large-scale scene recognition from abbey to zoo. In *2010 IEEE Conference on Computer Vision and Pattern Recognition*, pages 3485–3492. IEEE, 2010.
- [81] Y. Xu, Y. Chen, J. Nie, Y. Wang, H. Zhuang, and M. Okumura. Advancing cross-domain discriminability in continual learning of vision-language models. In *The Thirty-eighth Annual Conference on Neural Information Processing Systems*, 2024.
- [82] P. Yadav, D. Tam, L. Choshen, C. A. Raffel, and M. Bansal. Ties-merging: Resolving interference when merging models. *Advances in Neural Information Processing Systems*, 36: 7093–7115, 2023.
- [83] E. Yang, Z. Wang, L. Shen, S. Liu, G. Guo, X. Wang, and D. Tao. Adamerging: Adaptive model merging for multi-task learning. *arXiv preprint arXiv:2310.02575*, 2023.
- [84] E. Yang, L. Shen, Z. Wang, G. Guo, X. Chen, X. Wang, and D. Tao. Representation surgery for multi-task model merging. *Forty-first International Conference on Machine Learning*, 2024.
- [85] J. Yu, Y. Zhuge, L. Zhang, P. Hu, D. Wang, H. Lu, and Y. He. Boosting continual learning of vision-language models via mixture-of-experts adapters. In *Proceedings of the IEEE/CVF Conference on Computer Vision and Pattern Recognition*, pages 23219–23230, 2024.
- [86] L. Yu, B. Yu, H. Yu, F. Huang, and Y. Li. Language models are super mario: Absorbing abilities from homologous models as a free lunch. In *Forty-first International Conference on Machine Learning*, 2024.
- [87] L. Yuan, B. Xie, and S. Li. Robust test-time adaptation in dynamic scenarios. In *Proceedings of the IEEE/CVF Conference on Computer Vision and Pattern Recognition*, pages 15922–15932, 2023.

- [88] F. Zenke, B. Poole, and S. Ganguli. Continual learning through synaptic intelligence. *International conference on machine learning*, pages 3987–3995, 2017.
- [89] M. Zhang, S. Levine, and C. Finn. Memo: Test time robustness via adaptation and augmentation. *Advances in neural information processing systems*, 35:38629–38642, 2022.
- [90] Z. Zhao, L. Gan, G. Wang, W. Zhou, H. Yang, K. Kuang, and F. Wu. Loraretriever: Input-aware lora retrieval and composition for mixed tasks in the wild. In *Findings of the Association for Computational Linguistics ACL 2024*, pages 4447–4462, 2024.
- [91] Z. Zhao, T. Shen, D. Zhu, Z. Li, J. Su, X. Wang, and F. Wu. Merging loRAs like playing LEGO: Pushing the modularity of loRA to extremes through rank-wise clustering. In *The Thirteenth International Conference on Learning Representations*, 2025.
- [92] M. Zheng, Y. Tang, Z. Hao, K. Han, Y. Wang, and C. Xu. Adapt without forgetting: Distill proximity from dual teachers in vision-language models. In *European Conference on Computer Vision*, pages 109–125. Springer, 2024.
- [93] Z. Zheng, M. Ma, K. Wang, Z. Qin, X. Yue, and Y. You. Preventing zero-shot transfer degradation in continual learning of vision-language models. In *Proceedings of the IEEE/CVF international conference on computer vision*, pages 19125–19136, 2023.
- [94] D.-W. Zhou, H.-L. Sun, H.-J. Ye, and D.-C. Zhan. Expandable subspace ensemble for pre-trained model-based class-incremental learning. In *Proceedings of the IEEE/CVF Conference on Computer Vision and Pattern Recognition*, pages 23554–23564, 2024.

Appendix

The appendix is organized into sections, each providing additional information and details.

A	Theoretical Risk Comparison: Dynamic MoE vs. Static Averaging	16
B	Additional Descriptions	18
B.1	Details of Dataset and Task Settings	18
B.2	Details of Downstream Models	19
B.3	Details of Baselines	19
C	Additional Results	21
C.1	Detailed Overall Performance Results	21
C.2	Accuracy Trends Across Sequential Tasks	21
C.3	Detailed Results Under Distribution Shifts	25
C.4	More Visualizations of Gate Activations and Relaxation Effect	25
D	Discussions	27
D.1	Limitations	27
D.2	Broader Impacts	28

A Theoretical Risk Comparison: Dynamic MoE vs. Static Averaging

Problem Setup and Definitions Consider T independent tasks, each associated with a data distribution D_t for $t = 1, \dots, T$. For each task t , a pre-trained expert model $f_t(x)$ outputs a probability distribution over classes, trained specifically on D_t . The overall data distribution D is a mixture of these tasks, where an example (x, y) is drawn from task t with prior probability $P(t)$, and then $(x, y) \sim D_t$. The expected risk of a predictive model $h(x)$ is defined as:

$$R(h) = \mathbb{E}_{(x,y) \sim D} [\ell(h(x), y)] = \sum_{t=1}^T P(t) \mathbb{E}_{(x,y) \sim D_t} [\ell(h(x), y)], \quad (12)$$

where $\ell(h(x), y)$ is a loss function (e.g., cross-entropy or 0-1 loss).

We compare two methods to combine the experts into a final prediction $h(x)$:

- **Static Averaging:** Defined as $h_{\text{static}}(x) = \sum_{i=1}^T \alpha_i f_i(x)$, where $\alpha = (\alpha_1, \dots, \alpha_T)$ is a fixed weight vector independent of x , typically with $\alpha_i \geq 0$ and $\sum_i \alpha_i = 1$ for probability outputs.
- **Dynamic Mixture-of-Experts (MoE):** Defined as $h_{\text{MoE}}(x) = f_{i^*(x)}(x)$, where $i^*(x) = \arg \max_i g_i(x)$ and $g(x) = (g_1(x), \dots, g_T(x))$ is a gating function that selects one expert per input (hard routing). The gating is subject to routing noise, modeled below.

Routing Noise Model For each input x drawn from D_t , the true task is t , and the ideal expert is f_t . The gating selects the correct expert $i^*(x) = t$ with probability $1 - \varepsilon_t$, and an incorrect expert $i^*(x) \neq t$ with probability $\varepsilon_t = P(i^*(x) \neq t \mid x \sim D_t)$, the task-specific routing error rate. On error, the gating selects a random expert from $\{1, \dots, T\} \setminus \{t\}$ uniformly. Define:

- $R_t(i) = \mathbb{E}_{(x,y) \sim D_t} [\ell(f_i(x), y)]$, the risk of expert i on task t .
- $R_{\text{ideal}} = \sum_{t=1}^T P(t) R_t(t)$, the risk with perfect routing.
- $R_{\text{wrong},t} = \frac{1}{T-1} \sum_{i \neq t} R_t(i)$, the average risk of incorrect experts on task t .
- $\varepsilon = \sum_{t=1}^T P(t) \varepsilon_t$, the overall routing error rate.

Theorem 2 (Dynamic MoE versus Static Averaging). *Let $\{(D_t, f_t)\}_{t=1}^T$ be T independent tasks with priors $P(t)$ and per-task risks $R_t(i)$. For any static mixture $h_{\text{static}}(x) = \sum_{i=1}^T \alpha_i f_i(x)$ and any hard-routed MoE $h_{\text{MoE}}(x) = f_{i^*(x)}(x)$ with task-specific routing errors ε_t :*

$$R(h_{\text{MoE}}) = R_{\text{ideal}} + \sum_{t=1}^T P(t) \varepsilon_t (R_{\text{wrong},t} - R_t(t)), \quad (13)$$

where $R_{\text{ideal}} = \sum_t P(t)R_t(t)$ and $R_{\text{wrong},t} = \frac{1}{T-1} \sum_{i \neq t} R_t(i)$. Moreover,

1. (Perfect routing) If $\varepsilon_t = 0$ for all t , then $\inf_g R(h_{\text{MoE}}) < \inf_{\alpha} R(h_{\text{static}})$ whenever at least two tasks disagree on their best expert.
2. (Noisy routing) If $\sum_t P(t)\varepsilon_t(R_{\text{wrong},t} - R_t(t)) < R_{\text{static}}^* - R_{\text{ideal}}$, where $R_{\text{static}}^* = \inf_{\alpha} R(h_{\text{static}})$, then the MoE still attains lower risk than any static mixture.

Proof. The proof proceeds in three parts: (1) deriving the MoE risk with routing noise, (2) proving the optimal gating case, and (3) establishing the condition for MoE superiority under routing noise.

Step 1: MoE Risk with Routing Noise

The MoE prediction is $h_{\text{MoE}}(x) = f_{i^*(x)}(x)$, where $i^*(x) = \arg \max_i g_i(x)$. The expected risk is:

$$R(h_{\text{MoE}}) = \mathbb{E}_{(x,y) \sim D}[\ell(f_{i^*(x)}(x), y)] = \sum_{t=1}^T P(t) \mathbb{E}_{(x,y) \sim D_t}[\ell(f_{i^*(x)}(x), y)]. \quad (14)$$

For task t , condition on routing correctness:

- **Correct routing** ($i^*(x) = t$): Probability $1 - \varepsilon_t$, risk $R_t(t)$.
- **Incorrect routing** ($i^*(x) \neq t$): Probability ε_t , selects a random expert from $\{1, \dots, T\} \setminus \{t\}$, with average risk $R_{\text{wrong},t} = \frac{1}{T-1} \sum_{i \neq t} R_t(i)$.

The expected risk on task t is:

$$\mathbb{E}_{(x,y) \sim D_t}[\ell(f_{i^*(x)}(x), y)] = (1 - \varepsilon_t)R_t(t) + \varepsilon_t R_{\text{wrong},t}. \quad (15)$$

Thus, the total risk is:

$$R(h_{\text{MoE}}) = \sum_{t=1}^T P(t) [(1 - \varepsilon_t)R_t(t) + \varepsilon_t R_{\text{wrong},t}]. \quad (16)$$

Rewrite:

$$R(h_{\text{MoE}}) = \sum_{t=1}^T P(t)R_t(t) + \sum_{t=1}^T P(t)\varepsilon_t(R_{\text{wrong},t} - R_t(t)) = R_{\text{ideal}} + \sum_{t=1}^T P(t)\varepsilon_t\delta_t, \quad (17)$$

where $\delta_t = R_{\text{wrong},t} - R_t(t) > 0$ is the risk increase due to misrouting on task t .

Step 2: Optimal Gating (No Routing Noise)

Assume an oracle gating function with $\varepsilon_t = 0$ for all t , so $i^*(x) = t$ for all $x \sim D_t$. Then:

$$R(h_{\text{MoE}}) = \sum_{t=1}^T P(t)R_t(t) = R_{\text{ideal}}. \quad (18)$$

Define hypothesis classes:

$$\mathcal{H}_{\text{static}} = \left\{ x \mapsto \sum_{i=1}^T \alpha_i f_i(x) \mid \alpha \in \mathbb{R}^T \right\}, \quad (19)$$

$$\mathcal{H}_{\text{MoE}} = \left\{ x \mapsto f_{i^*(x)}(x) \mid i^*(x) = \arg \max_i g_i(x), g : \mathcal{X} \rightarrow \mathbb{R}^T \right\}. \quad (20)$$

Any static model $h_{\text{static}}(x) = \sum_{i=1}^T \alpha_i f_i(x)$ can be approximated by an MoE with $g(x)$ assigning constant weights, so $\mathcal{H}_{\text{static}} \subseteq \mathcal{H}_{\text{MoE}}$. Thus:

$$R_{\text{MoE}}^* = \inf_{g(\cdot)} R(h_{\text{MoE}}) \leq \inf_{\alpha} R(h_{\text{static}}) = R_{\text{static}}^*. \quad (21)$$

Under task heterogeneity ($R_t(t) < R_t(s)$ and $R_s(s) < R_s(t)$ for some $t \neq s$), the ideal MoE routes each $x \sim D_t$ to f_t , achieving:

$$R_{\text{ideal}} = \sum_{t=1}^T P(t)R_t(t). \quad (22)$$

For static averaging:

$$R(h_{\text{static}}) = \sum_{t=1}^T P(t)\mathbb{E}_{(x,y) \sim D_t} \left[\ell \left(\sum_{i=1}^T \alpha_i f_i(x), y \right) \right]. \quad (23)$$

Since ℓ is convex (e.g., cross-entropy), Jensen’s inequality implies:

$$\mathbb{E}_{D_t} \left[\ell \left(\sum_i \alpha_i f_i(x), y \right) \right] \geq R_t(t), \quad (24)$$

with strict inequality unless $\alpha_t = 1$ and $\alpha_i = 0$ for $i \neq t$, which cannot hold for all tasks simultaneously under heterogeneity. Thus:

$$R_{\text{static}}^* > R_{\text{ideal}} = R_{\text{MoE}}^*. \quad (25)$$

Step 3: MoE Superiority with Routing Noise

Let $\gamma = R_{\text{static}}^* - R_{\text{ideal}} > 0$ under task heterogeneity. The MoE outperforms the static model if:

$$R(h_{\text{MoE}}) < R_{\text{static}}^*. \quad (26)$$

Substitute:

$$R_{\text{ideal}} + \sum_{t=1}^T P(t)\varepsilon_t\delta_t < R_{\text{ideal}} + \gamma. \quad (27)$$

Thus:

$$\sum_{t=1}^T P(t)\varepsilon_t\delta_t < \gamma = R_{\text{static}}^* - R_{\text{ideal}}. \quad (28)$$

Since $\delta_t = R_{\text{wrong},t} - R_t(t)$, the condition is:

$$\sum_{t=1}^T P(t)\varepsilon_t(R_{\text{wrong},t} - R_t(t)) < R_{\text{static}}^* - R_{\text{ideal}}. \quad (29)$$

If this holds, the MoE’s risk, despite routing noise, remains below the best static risk. \square

Conclusion: The MoE risk is $R_{\text{ideal}} + \sum_{t=1}^T P(t)\varepsilon_t(R_{\text{wrong},t} - R_t(t))$, and it outperforms static averaging when routing noise is sufficiently small relative to the static model’s suboptimality. The optimal gating case confirms $R_{\text{MoE}}^* \leq R_{\text{static}}^*$, with strict inequality under task heterogeneity.

B Additional Descriptions

B.1 Details of Dataset and Task Settings

Dataset Details Following prior works [68], we evaluate continual model merging on twenty publicly available image classification datasets, including SUN397 [80], Stanford Cars [31], RE-SISC45 [4], EuroSAT [18], SVHN [44], GTSRB [62], MNIST [33], DTD [6], Flowers102 [45], PCAM [71], FER2013 [17], Oxford-IIIT Pet [48], STL-10 [8], CIFAR-100 and CIFAR-10 [32], Food-101 [3], Fashion-MNIST [79], EMNIST [9], KMNIST [7], and Rendered SST-2 [60].

Table 6: Extended downstream datasets used in our experiments.

Dataset	#Classes	#Train (k)	#Test (k)	Task
SUN397	287	19.9	19.9	Scene category
Stanford Cars	196	8.1	8.0	Car series
RESISC45	45	18.9	6.3	Remote-sensing scene
EuroSAT	10	21.6	2.7	Satellite land-use
SVHN	10	73.3	26.0	Digit recognition
GTSRB	43	39.2	12.6	Traffic sign
MNIST	10	60	10	Hand-written digit
DTD	47	3.8	1.9	Texture recognition
Flowers102	102	1.0	6.1	Flower species
PCAM	2	262	32.8	Tumour detection
FER2013	7	28.7	3.6	Facial emotion
Oxford IIIT Pet	37	3.7	3.7	Animal species
STL10	10	5	8	Object recognition
CIFAR-100	100	50	10	Natural object
CIFAR-10	10	50	10	Natural object
Food101	101	75.8	25.3	Food type
Fashion-MNIST	10	60	10	Fashion product
EMNIST (digits)	10	60	10	Hand-written digit
KMNIST	10	60	10	Kuzushiji character
Rendered SST-2	2	6.9	1.8	Rendered sentiment

Task Grouping We group the 20 datasets into three progressive task sets and evaluate the merged models using average accuracy (ACC) and backward transfer (BWT) metrics. For each task group, we perform 10 experiments using different task sequences (listed in Tab. 7), and report both the mean and standard deviation of the results to ensure robustness and consistency.

- **8-task group:** (1) SUN397, (2) Stanford Cars, (3) RESISC45, (4) EuroSAT, (5) SVHN, (6) GTSRB, (7) MNIST, (8) DTD.
- **14-task group:** (1) SUN397, (2) Stanford Cars, (3) RESISC45, (4) EuroSAT, (5) SVHN, (6) GTSRB, (7) MNIST, (8) DTD, (9) Flowers102, (10) PCAM, (11) FER2013, (12) OxfordIIITPet, (13) STL10, (14) CIFAR100.
- **20-task group:** (1) SUN397, (2) Stanford Cars, (3) RESISC45, (4) EuroSAT, (5) SVHN, (6) GTSRB, (7) MNIST, (8) DTD, (9) Flowers102, (10) PCAM, (11) FER2013, (12) OxfordIIITPet, (13) STL10, (14) CIFAR100, (15) CIFAR10, (16) Food101, (17) FashionMNIST, (18) EMNIST, (19) KMNIST, (20) RenderedSST2.

B.2 Details of Downstream Models

In this section, we present the evaluation setup for pre-trained and fine-tuned models. As shown in Tab. 8, we evaluate the zero-shot accuracy of the original CLIP-ViT models and the performance of fine-tuned models on the test sets of various downstream tasks. The fine-tuned checkpoints are obtained directly from Hugging Face (<https://huggingface.co/tanganke>), where each model has been fine-tuned on task-specific training data using a standard protocol. The visual encoder is updated during fine-tuning, while the classification head is fixed and initialized from the pre-trained text encoder. The fine-tuning setup follows a standard configuration: cross-entropy loss, Adam optimizer, cosine annealing learning rate schedule with a peak learning rate of 1e-5, batch size 128, and 4000 training steps.

B.3 Details of Baselines

Our experiments involve the following comparison methods and our method:

- **Stochastic Weight Averaging (SWA).** A simple model averaging technique to stabilize optimization and improve generalization [25]. At each step t , the model parameters are averaged across previous checkpoint: $\theta_t^{\text{SWA}} = \frac{1}{t} [\theta_{t-1}^{\text{SWA}}(t-1) + \theta_t^{\text{SWA}}]$. This approach can be interpreted

Table 7: Dataset orderings used for experiments in each task group.

Group	Order	Dataset Order (by ID)
8 tasks	1	(04 → 05 → 07 → 08 → 03 → 06 → 01 → 02)
	2	(07 → 08 → 05 → 04 → 02 → 06 → 03 → 01)
	3	(03 → 06 → 04 → 02 → 01 → 08 → 05 → 07)
	4	(06 → 08 → 02 → 01 → 03 → 07 → 04 → 05)
	5	(07 → 06 → 03 → 08 → 05 → 01 → 04 → 02)
	6	(07 → 02 → 03 → 08 → 05 → 04 → 01 → 06)
	7	(07 → 01 → 04 → 03 → 08 → 05 → 02 → 06)
	8	(08 → 05 → 06 → 07 → 01 → 04 → 03 → 02)
	9	(01 → 04 → 05 → 02 → 06 → 03 → 07 → 08)
	10	(08 → 03 → 01 → 02 → 06 → 05 → 07 → 04)
14 tasks	1	(09 → 13 → 08 → 07 → 14 → 12 → 06 → 03 → 10 → 04 → 05 → 01 → 02 → 11)
	2	(09 → 10 → 11 → 14 → 07 → 13 → 04 → 02 → 06 → 08 → 03 → 12 → 05 → 01)
	3	(05 → 08 → 12 → 06 → 11 → 01 → 10 → 04 → 14 → 03 → 02 → 13 → 09 → 07)
	4	(03 → 10 → 09 → 12 → 04 → 13 → 01 → 06 → 11 → 02 → 14 → 08 → 07 → 05)
	5	(08 → 14 → 09 → 06 → 12 → 13 → 05 → 03 → 04 → 11 → 10 → 01 → 07 → 02)
	6	(03 → 12 → 13 → 01 → 11 → 04 → 10 → 05 → 14 → 08 → 09 → 07 → 02 → 06)
	7	(07 → 01 → 12 → 10 → 02 → 08 → 13 → 04 → 05 → 11 → 14 → 03 → 06 → 09)
	8	(05 → 12 → 04 → 11 → 03 → 08 → 10 → 01 → 09 → 13 → 14 → 07 → 06 → 02)
	9	(10 → 07 → 09 → 02 → 03 → 13 → 01 → 12 → 14 → 04 → 11 → 06 → 05 → 08)
	10	(01 → 02 → 11 → 06 → 08 → 12 → 07 → 05 → 10 → 14 → 03 → 13 → 09 → 04)
20 tasks	1	(20 → 06 → 15 → 05 → 10 → 14 → 16 → 19 → 07 → 13 → 18 → 11 → 02 → 12 → 03 → 17 → 08 → 09 → 01 → 04)
	2	(09 → 14 → 06 → 03 → 07 → 04 → 18 → 01 → 17 → 19 → 08 → 20 → 13 → 16 → 11 → 12 → 15 → 05 → 10 → 02)
	3	(09 → 15 → 16 → 11 → 03 → 13 → 08 → 10 → 12 → 02 → 20 → 01 → 05 → 19 → 07 → 06 → 04 → 18 → 17 → 14)
	4	(17 → 04 → 11 → 19 → 18 → 10 → 07 → 15 → 12 → 13 → 08 → 02 → 01 → 06 → 05 → 03 → 20 → 16 → 14 → 09)
	5	(14 → 16 → 04 → 20 → 15 → 17 → 07 → 11 → 06 → 18 → 12 → 01 → 19 → 09 → 10 → 05 → 08 → 02 → 13 → 03)
	6	(02 → 06 → 17 → 04 → 19 → 18 → 08 → 16 → 20 → 01 → 10 → 13 → 07 → 09 → 05 → 11 → 15 → 14 → 03 → 12)
	7	(19 → 01 → 09 → 14 → 06 → 20 → 17 → 04 → 08 → 02 → 15 → 03 → 16 → 13 → 12 → 07 → 10 → 05 → 11 → 18)
	8	(15 → 07 → 08 → 02 → 10 → 06 → 17 → 20 → 05 → 19 → 16 → 01 → 18 → 09 → 13 → 11 → 04 → 14 → 12 → 03)
	9	(10 → 05 → 07 → 11 → 01 → 03 → 17 → 15 → 18 → 04 → 14 → 19 → 02 → 06 → 13 → 20 → 08 → 12 → 09 → 16)
	10	(01 → 11 → 02 → 15 → 03 → 10 → 12 → 19 → 16 → 13 → 07 → 05 → 09 → 04 → 14 → 20 → 06 → 18 → 17 → 08)

as a form of uniform model ensembling. While conceptually straightforward, SWA treats all checkpoints equally and does not account for inter-task conflicts.

- Continual Task Arithmetic (C. TA).** A training-free merging strategy that linearly combines task-specific fine-tuned models with a shared pre-trained model [23]. It computes the merged parameters as $\theta_t^{\text{merged}} = \theta_{t-1}^{\text{merged}} + \lambda(\theta_t - \theta_0)$, where λ is a scaling factor. TA is computationally efficient and easy to apply, but sensitive to λ and prone to destructive interference when merging dissimilar tasks.
- Continual Ties-Merging (C. Ties).** An extension of Task Arithmetic that reduces parameter-level redundancy and sign conflicts during model merging [82]. For task t , the difference vector $\Delta\theta_t = \theta_t - \theta_0$ is trimmed and sign-normalized to obtain $\Delta\theta_t^{\text{Ties}} = \text{Ties}(\Delta\theta_{t-1}^{\text{Ties}}, \Delta\theta_t)$, and the merged model is given by $\theta_t^{\text{merged}} = \theta_{t-1}^{\text{merged}} + \lambda\Delta\theta_t^{\text{Ties}}$.
- Orthogonal Projection-based Continual Merging (OPCM).** A projection-based scheme to mitigate task interference by enforcing orthogonality between parameter updates [68]. Specifically, each $\Delta\theta_t$ is projected onto the orthogonal complement of the subspace spanned by previous updates: $\theta_t^{\text{merged}} = \theta_0 + \frac{1}{\lambda_t} \left[\lambda_{t-1} \Delta\theta_{t-1}^{\text{merged}} + \mathcal{P}^{(t-1)}(\Delta\theta_t) \right]$, where $\mathcal{P}^{(t-1)}$ denotes the orthogonal projection.
- Maximum Magnitude Selection (MagMax).** An extension of Task Arithmetic that, for each parameter dimension, selects the update with the larger absolute value: $\Delta\theta_t^{\text{MagMax}} = \text{MagMax}(\Delta\theta_{t-1}^{\text{MagMax}}, \Delta\theta_t)$, and the merged model is given by $\theta_t^{\text{merged}} = \theta_{t-1}^{\text{merged}} + \lambda\Delta\theta_t^{\text{MagMax}}$.

Table 8: Test set accuracy of the pre-trained model and individual fine-tuned models on different downstream tasks.

Model	SUN397	Cars	RESISC45	EuroSAT	SVHN	GTSRB	MNIST	DTD	Flowers102	PCAM
CLIP-ViT-B/32										
Pre-trained	63.2	59.6	60.3	45.0	31.6	32.5	48.3	44.2	66.4	60.6
Fine-tuned	74.9	78.5	95.1	99.1	97.3	98.9	99.6	79.7	88.6	88.0
CLIP-ViT-B/16										
Pre-trained	65.5	64.7	66.4	54.1	52.0	43.5	51.7	45.0	71.3	54.0
Fine-tuned	78.9	85.9	96.6	99.0	97.6	99.0	99.7	82.3	94.9	90.6
CLIP-ViT-L/14										
Pre-trained	68.2	77.9	71.3	61.2	58.4	50.5	76.3	55.5	79.2	51.2
Fine-tuned	82.8	92.8	97.4	99.1	97.9	99.2	99.8	85.5	97.7	91.1

Model	FER2013	OxfordIIITPet	STL10	CIFAR-100	CIFAR-10	Food101	FashionMNIST	EMNIST	KMNIST	RenderedSST2
CLIP-ViT-B/32										
Pre-trained	41.3	83.3	97.1	63.7	89.8	82.4	63.0	12.0	10.0	58.6
Fine-tuned	71.6	92.5	97.5	88.4	97.6	88.4	94.7	95.6	98.2	71.3
CLIP-ViT-B/16										
Pre-trained	46.4	88.4	98.3	66.3	90.8	87.0	67.3	12.4	11.2	60.6
Fine-tuned	72.8	94.5	98.2	88.8	98.3	91.9	94.5	95.3	98.1	75.7
CLIP-ViT-L/14										
Pre-trained	50.0	93.2	99.4	75.1	95.6	91.2	67.0	12.3	9.7	68.9
Fine-tuned	75.9	95.7	99.2	93.0	99.1	94.8	95.3	95.4	98.3	80.5

C Additional Results

In this section, we provide additional experimental results to support the findings reported in the main paper. Specifically, we include: (1) detailed overall performance results (C.1); (2) accuracy trends across sequential tasks (C.2); (3) detailed results under distribution shifts (C.3); and (4) extended visualizations of gate activations and hyperparameter effects (C.4).

C.1 Detailed Overall Performance Results

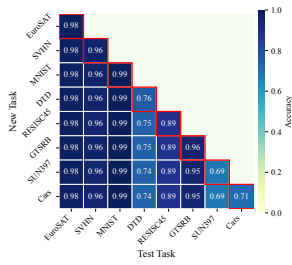
Tab. 9 expands on the average results in Tab. 1 by reporting per-task average accuracy after continually merging 20 tasks. We compare six methods, SWA, Task Arithmetic, Ties-Merging, MagMax-IND, OPCM, and our proposed MINGLE across three CLIP-ViT backbones (B/32, B/16, L/14). MINGLE achieves the highest accuracy on most tasks. These fine-grained results reinforce the main paper’s findings, highlighting MINGLE’s ability to improve performance on continual model merging.

C.2 Accuracy Trends Across Sequential Tasks

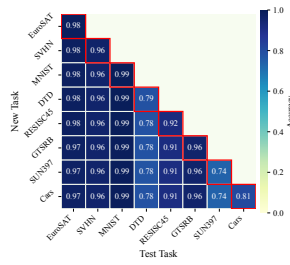
Fig. 6 provides a detailed view of accuracy throughout the continual merging process across different settings, showing both the performance on the current task and on previously encountered ones. The progressive accuracy drop across columns illustrates the degree of forgetting over time. Notably, MINGLE consistently alleviates this degradation, demonstrating markedly reduced forgetting across the full task sequence. Fig. 7 further compares the average accuracy curves of MINGLE and baseline methods on previously seen tasks after each new model is merged, using the CLIP ViT-B/16 backbone. Results are averaged over 10 random task orderings. MINGLE consistently achieves the highest performance throughout the merging process, with its accuracy curve clearly dominating those of competing methods. Moreover, the narrower standard deviation bands indicate that MINGLE is more robust to the task orders.

Table 9: Test set accuracy comparisons on different downstream tasks.

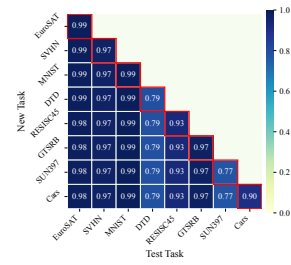
Model	SUN397	Cars	RESISC45	EuroSAT	SVHN	GTSRB	MNIST	DTD	Flowers102	PCAM
ViT-B/32										
C. FINE-TUNED	53.9	38.2	64.7	98.7	45.4	34.4	86.7	58.4	57.5	67.7
AVERAGE (SWA)	64.2	59.6	64.8	60.9	47.3	43.1	71.8	46.4	66.5	63.9
C.TA	62.0	53.7	60.9	58.1	48.5	48.9	79.4	46.1	61.1	73.4
C.TIES	62.5	49.1	55.8	50.9	54.6	49.3	82.0	46.7	58.5	69.9
MAGMAX-IND	63.6	53.1	59.7	49.1	53.8	53.1	79.8	43.2	56.9	75.1
OPCM	64.4	51.1	66.0	71.7	66.1	56.0	90.2	40.4	64.9	80.2
MINGLE (OURS)	67.8	58.3	83.5	90.0	82.9	91.8	98.0	65.3	74.0	66.9
ViT-B/16										
C. FINE-TUNED	62.7	58.0	67.6	99.1	46.0	29.2	93.9	61.9	64.1	75.2
AVERAGE (SWA)	67.1	64.6	69.3	63.4	62.4	52.7	80.7	46.6	71.8	63.1
C.TA	65.8	57.5	63.8	59.5	64.7	54.0	88.0	45.3	67.5	67.1
C.TIES	64.2	52.9	60.9	53.0	62.8	48.8	88.4	45.0	61.3	68.5
MAGMAX-IND	65.8	51.8	57.8	42.6	54.4	43.7	83.0	42.8	60.4	69.8
OPCM	67.9	55.9	73.7	77.5	74.4	63.2	94.1	49.2	72.3	79.6
MINGLE (OURS)	71.9	64.4	83.0	84.7	83.8	85.3	92.3	60.7	83.5	77.7
ViT-L/14										
C. FINE-TUNED	69.5	73.6	78.3	99.2	59.3	49.3	98.6	69.7	83.2	78.3
AVERAGE (SWA)	70.7	77.7	76.4	75.3	69.5	62.1	93.7	57.7	80.0	73.6
C.TA	70.4	74.1	73.9	66.3	69.9	65.6	95.1	56.6	78.6	70.4
C.TIES	69.7	70.3	65.3	47.9	76.1	63.6	94.7	54.4	77.9	72.3
MAGMAX-IND	73.1	73.7	75.6	64.6	73.7	68.8	94.6	56.1	78.0	71.7
OPCM	73.1	78.3	82.4	80.2	80.8	80.4	97.4	61.6	84.8	76.3
MINGLE (OURS)	74.5	85.9	90.5	92.5	90.1	92.7	98.1	69.2	95.7	74.0
ViT-B/32										
C. FINE-TUNED	58.3	68.5	86.7	40.2	70.5	50.0	90.7	72.4	54.5	54.5
AVERAGE (SWA)	50.2	84.1	97.0	69.8	92.7	80.4	71.3	15.0	11.5	61.8
C.TA	51.4	82.3	94.9	64.6	91.4	71.9	73.9	17.8	12.2	59.9
C.TIES	49.5	81.3	95.2	63.7	91.2	70.2	73.7	17.8	16.9	59.8
MAGMAX-IND	56.5	79.9	94.6	68.7	91.9	73.8	74.3	18.3	15.4	63.9
OPCM	55.8	82.9	95.9	67.6	92.8	74.0	76.3	22.4	18.3	64.6
MINGLE (OURS)	65.0	85.5	97.0	72.6	94.1	81.5	85.4	50.4	65.2	67.1
ViT-B/16										
C. FINE-TUNED	60.5	84.5	90.5	38.8	73.6	61.9	89.7	83.3	51.5	72.8
AVERAGE (SWA)	50.9	89.6	98.0	72.9	94.2	85.9	73.3	15.6	12.4	62.5
C.TA	50.7	89.3	97.0	68.0	93.1	80.3	75.7	18.1	16.7	61.8
C.TIES	50.4	87.9	96.3	63.1	91.7	78.0	75.0	23.4	24.9	61.5
MAGMAX-IND	57.7	88.8	97.5	71.5	94.4	81.3	77.2	24.5	25.0	59.4
OPCM	59.5	91.8	97.7	73.2	94.7	83.1	81.3	26.5	23.4	66.8
MINGLE (OURS)	65.1	92.2	97.4	74.3	94.8	87.3	84.8	67.1	81.7	71.7
ViT-L/14										
C. FINE-TUNED	68.0	92.1	94.5	60.5	85.7	74.8	93.1	89.0	59.2	78.8
AVERAGE (SWA)	52.7	94.2	99.2	81.7	97.0	90.7	77.4	16.1	10.4	66.1
C.TA	55.7	94.2	98.6	79.1	91.6	87.6	80.8	17.6	10.6	63.6
C.TIES	57.6	93.5	97.8	74.0	95.6	84.7	79.7	20.2	12.6	58.4
MAGMAX-IND	52.9	93.9	98.7	82.1	97.3	89.5	81.6	19.2	11.1	68.4
OPCM	61.8	95.4	99.2	83.0	97.8	90.9	86.0	26.4	14.7	71.0
MINGLE (OURS)	67.9	96.0	99.4	84.7	97.8	92.4	88.8	53.0	57.1	75.5
ViT-B/32										
C. FINE-TUNED	58.3	68.5	86.7	40.2	70.5	50.0	90.7	72.4	54.5	54.5
AVERAGE (SWA)	50.2	84.1	97.0	69.8	92.7	80.4	71.3	15.0	11.5	61.8
C.TA	51.4	82.3	94.9	64.6	91.4	71.9	73.9	17.8	12.2	59.9
C.TIES	49.5	81.3	95.2	63.7	91.2	70.2	73.7	17.8	16.9	59.8
MAGMAX-IND	56.5	79.9	94.6	68.7	91.9	73.8	74.3	18.3	15.4	63.9
OPCM	55.8	82.9	95.9	67.6	92.8	74.0	76.3	22.4	18.3	64.6
MINGLE (OURS)	65.0	85.5	97.0	72.6	94.1	81.5	85.4	50.4	65.2	67.1
ViT-B/16										
C. FINE-TUNED	60.5	84.5	90.5	38.8	73.6	61.9	89.7	83.3	51.5	72.8
AVERAGE (SWA)	50.9	89.6	98.0	72.9	94.2	85.9	73.3	15.6	12.4	62.5
C.TA	50.7	89.3	97.0	68.0	93.1	80.3	75.7	18.1	16.7	61.8
C.TIES	50.4	87.9	96.3	63.1	91.7	78.0	75.0	23.4	24.9	61.5
MAGMAX-IND	57.7	88.8	97.5	71.5	94.4	81.3	77.2	24.5	25.0	59.4
OPCM	59.5	91.8	97.7	73.2	94.7	83.1	81.3	26.5	23.4	66.8
MINGLE (OURS)	65.1	92.2	97.4	74.3	94.8	87.3	84.8	67.1	81.7	71.7
ViT-L/14										
C. FINE-TUNED	68.0	92.1	94.5	60.5	85.7	74.8	93.1	89.0	59.2	78.8
AVERAGE (SWA)	52.7	94.2	99.2	81.7	97.0	90.7	77.4	16.1	10.4	66.1
C.TA	55.7	94.2	98.6	79.1	91.6	87.6	80.8	17.6	10.6	63.6
C.TIES	57.6	93.5	97.8	74.0	95.6	84.7	79.7	20.2	12.6	58.4
MAGMAX-IND	52.9	93.9	98.7	82.1	97.3	89.5	81.6	19.2	11.1	68.4
OPCM	61.8	95.4	99.2	83.0	97.8	90.9	86.0	26.4	14.7	71.0
MINGLE (OURS)	67.9	96.0	99.4	84.7	97.8	92.4	88.8	53.0	57.1	75.5



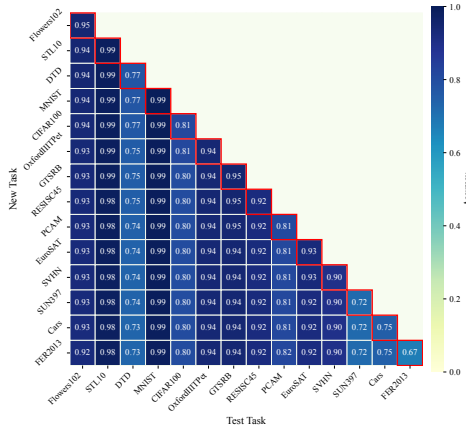
(a) ViT-B/32 on 8 Tasks



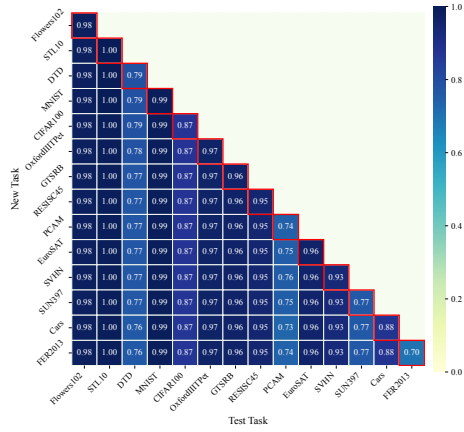
(b) ViT-B/16 on 8 Tasks



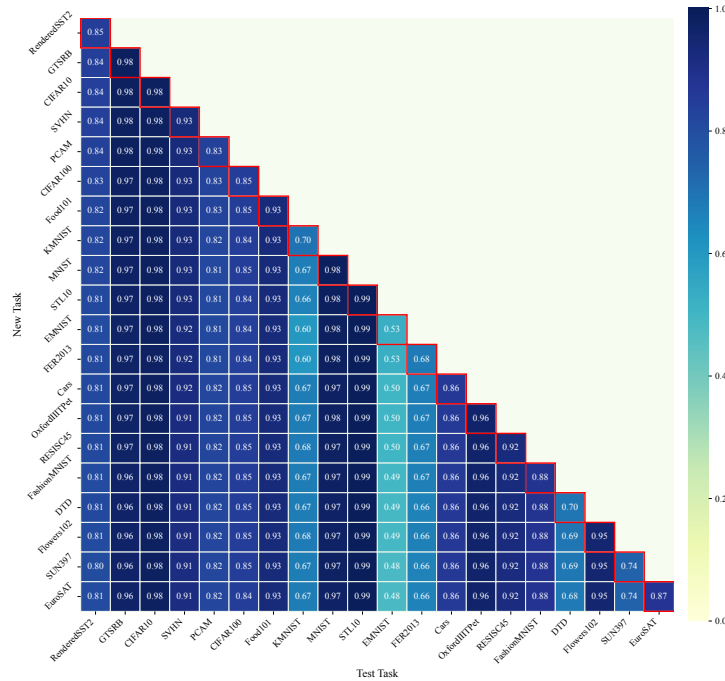
(c) ViT-L/14 on 8 Tasks



(d) ViT-B/16 on 14 Tasks

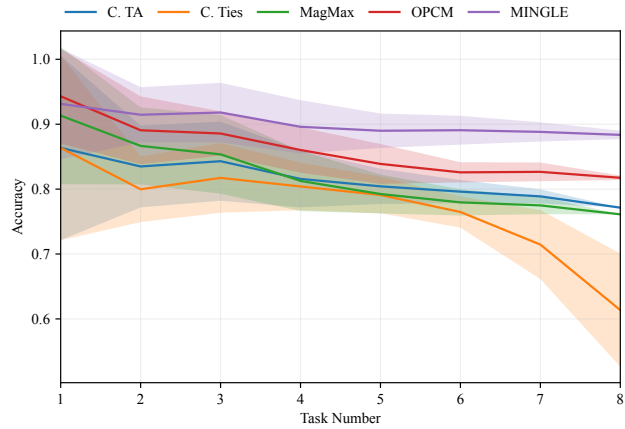


(e) ViT-L/14 on 14 Tasks

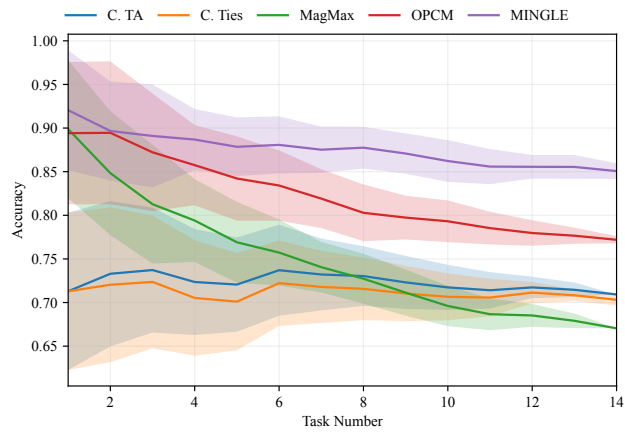


(f) ViT-L/14 on 20 Tasks

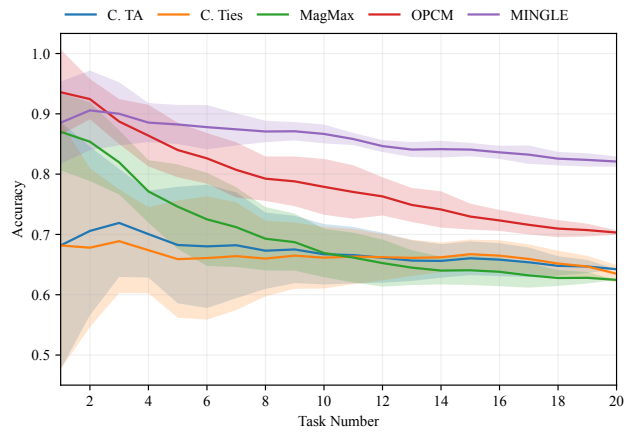
Figure 6: Accuracy matrices of MINGLE (ViT-B/32, ViT-B/16, and ViT-L/14) under different task settings.



(a) 8 tasks



(b) 14 tasks



(c) 20 tasks

Figure 7: Sequential test accuracy curves of MINGLE and baselines (C.TA, C.Ties, MagMax, OPCM) under different task settings. Shaded regions indicate standard deviation across 10 task orders.

Table 10: Robustness results when merging ViT-B/32 models on four tasks.

Method	Clean Test Set					Corruption: Motion Blur				
	Cars	EuroSAT	RESISC45	GTSRB	Avg ACC	Cars	EuroSAT	RESISC45	GTSRB	Avg ACC
C. LW ADAMERGING	65.3	49.7	65.4	43.8	56.0	64.2	25.6	62.5	37.5	47.5
C. WEMOE	0.5	8.1	2.6	2.5	3.4	0.5	8.0	1.8	2.3	3.2
C. TASK ARITHMETIC	64.6	90.4	80.2	74.8	77.5	62.3	59.4	78.5	63.3	65.9
MAGMAX-IND	63.1	89.2	81.7	82.5	79.1	61.4	62.1	80.0	72.6	69.0
OPCM	65.7	92.3	85.7	90.5	83.6	62.8	62.5	83.7	82.2	72.8
MINGLE	74.4	96.5	91.5	97.3	89.9	73.2	70.5	91.9	95.8	82.9
Method	Corruption: Impulse Noise					Corruption: Gaussian Noise				
	Cars	EuroSAT	RESISC45	GTSRB	Avg ACC	Cars	EuroSAT	RESISC45	GTSRB	Avg ACC
C. LW ADAMERGING	60.5	30.1	56.3	25.5	43.1	62.3	25.6	59.7	25.6	43.3
C. WEMOE	0.5	11.2	2.3	3.2	4.3	0.5	8.1	2.4	2.8	3.4
C. TASK ARITHMETIC	59.9	57.7	72.9	45.0	58.9	61.8	51.4	75.1	50.1	59.6
MAGMAX-IND	59.2	56.3	74.3	52.5	60.6	60.6	51.7	77.0	56.5	61.5
OPCM	61.1	57.1	78.5	62.0	64.7	63.0	52.4	80.7	64.9	65.2
MINGLE	69.6	28.0	86.1	86.1	67.5	72.0	38.5	89.4	82.9	70.7
Method	Corruption: Pixelate					Corruption: Spatter				
	Cars	EuroSAT	RESISC45	GTSRB	Avg ACC	Cars	EuroSAT	RESISC45	GTSRB	Avg ACC
C. LW ADAMERGING	3.4	16.5	13.5	39.2	18.1	61.3	34.1	58.2	32.8	46.6
C. WEMOE	0.5	6.3	2.5	2.5	3.0	0.5	10.1	2.7	2.6	4.0
C. TASK ARITHMETIC	2.5	31.7	19.1	65.6	29.7	61.2	63.1	72.7	57.0	63.5
MAGMAX-IND	2.6	36.1	19.3	74.0	33.0	60.0	64.9	74.8	66.1	66.4
OPCM	2.1	34.3	19.5	84.9	35.2	61.5	64.7	78.8	76.8	70.5
MINGLE	2.3	35.6	18.5	95.1	37.9	70.1	57.8	86.2	93.9	77.0
Method	Corruption: Contrast					Corruption: JPEG Compression				
	Cars	EuroSAT	RESISC45	GTSRB	Avg ACC	Cars	EuroSAT	RESISC45	GTSRB	Avg ACC
C. LW ADAMERGING	61.8	26.0	63.1	44.8	48.9	65.1	29.6	65.4	36.4	49.1
C. WEMOE	0.5	7.5	2.3	3.0	3.3	0.5	10.5	2.4	2.7	4.0
C. TASK ARITHMETIC	62.5	55.2	75.3	70.8	66.0	64.1	66.2	80.0	61.0	67.8
MAGMAX-IND	61.3	58.0	76.9	78.2	68.6	62.5	67.7	81.1	68.5	69.9
OPCM	63.8	57.5	81.3	87.4	72.5	65.0	68.0	85.4	79.3	74.4
MINGLE	72.4	60.1	90.4	97.3	80.1	73.7	73.5	92.0	92.4	82.9

C.3 Detailed Results Under Distribution Shifts

Tab. 10 expands on Tab. 2 by reporting per-dataset accuracy under both clean test conditions and seven common corruption types: motion blur, impulse noise, Gaussian noise, pixelation, spatter, contrast shift, and JPEG compression. We evaluate six merging methods, across four downstream tasks: Cars, EuroSAT, RESISC45, and GTSRB. This detailed breakdown complements the average results in the main paper, providing a more comprehensive assessment of robustness under test-time distribution shifts.

C.4 More Visualizations of Gate Activations and Relaxation Effect

We provide an extended ablation study on gate hyper-parameters, including visualizations of gate activations under 14-task (Fig. 8) and 20-task (Fig. 9) configurations, complementing the 8-task results presented in the main paper. The visualizations demonstrate that the null-space constraint remains effective as the number of tasks increases, consistently suppressing gate responses to inputs from previously seen tasks and thereby mitigating forgetting.

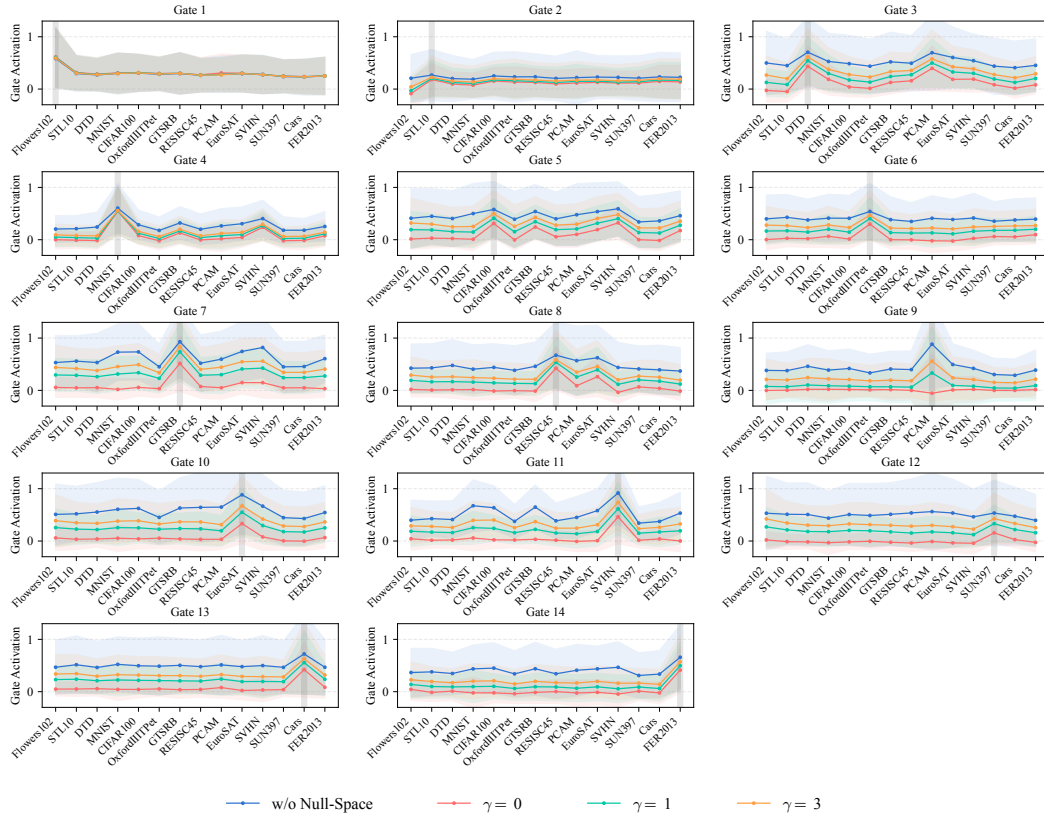


Figure 8: Visualization of gate activations across 14 tasks under varying γ values. Each subplot corresponds to a gate, with curves and shaded regions denoting the mean and standard deviation of activations across layers. Gray bars mark the training dataset for each gate. Smaller γ values result in stronger suppression of activations on previously learned tasks.

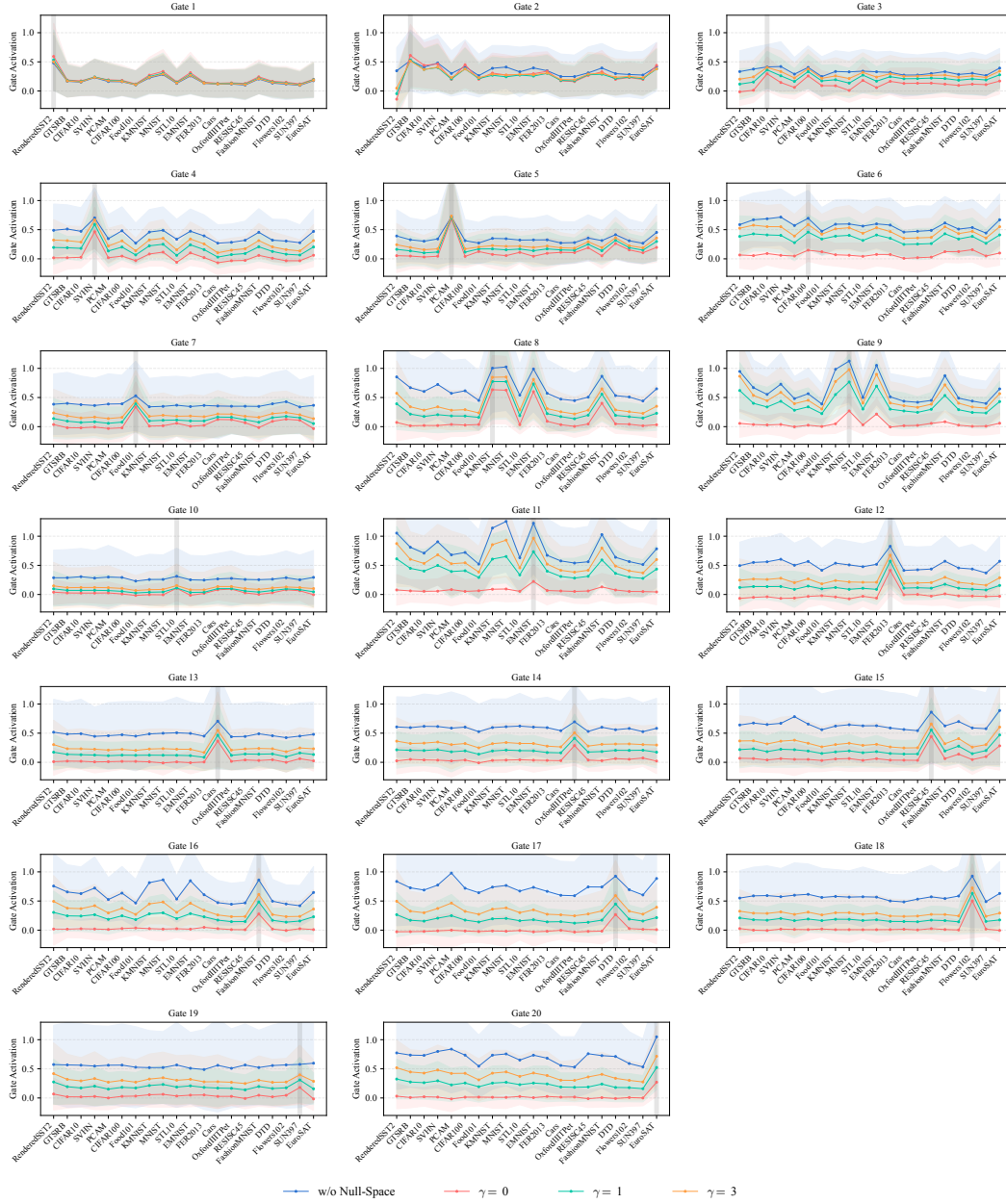


Figure 9: Visualization of gate activations across 20 tasks under varying γ values.

D Discussions

D.1 Limitations

As with many model merging methods, our approach assumes that all independently fine-tuned models originate from a shared pretrained initialization. The extent to which this assumption influences merging performance remains unclear and warrants further investigation. In addition, our current experiments focus on merging models with identical backbone architectures (*e.g.*, CLIP ViT-B/16). Although our use of LoRA-based expert offers some structural uniformity, which could potentially accommodate heterogeneous backbones, we have not yet explored this setting. Extending our framework to support diverse initialization points or architectural variants remains an open direction for future work.

D.2 Broader Impacts

This paper presents work whose goal is to advance the field of Machine Learning. There are many potential societal consequences of our work, none which we feel must be specifically highlighted here.